

NO-A004 031

WESTINGHOUSE ELECTRIC CORP PITTSBURGH PA

F/G 10/2

RIBBON GROWTH OF SINGLE CRYSTAL GAAS FOR SOLAR CELL APPLICATION--ETC(U)

NOV 79 T A GOULD, R G SEIDENSTICKER

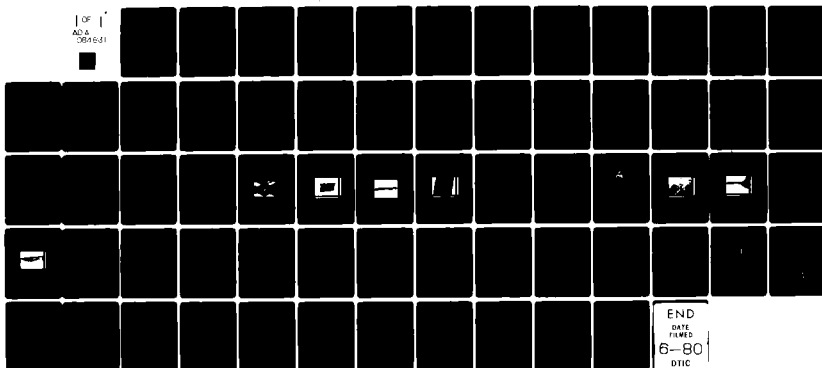
F33615-78-C-2031

UNCLASSIFIED

AFAPL-TR-79-2094

NL

1 OF 1  
AD-A  
0815-01



END  
DATE  
FILMED  
6-80  
DTIC

ADA 084831

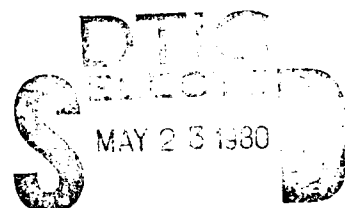
AFAPL-TR-79-2094

RIBBON GROWTH OF SINGLE CRYSTAL GaAs FOR  
SOLAR CELL APPLICATION

WESTINGHOUSE ELECTRIC CORPORATION  
1310 BEULAH ROAD  
PITTSBURGH PA 15235

NOVEMBER 1979

TECHNICAL REPORT AFAPL-TR-79-2094  
Interim Technical Report; 15 August 1978 - 15 August 1979



A

DDC FILE COPY

Approved for public release; distribution unlimited

AIR FORCE AERO PROPULSION LABORATORY  
AIR FORCE WRIGHT AERONAUTICAL LABORATORIES  
AIR FORCE SYSTEMS COMMAND  
WRIGHT-PATTERSON AIR FORCE BASE, OHIO 45433

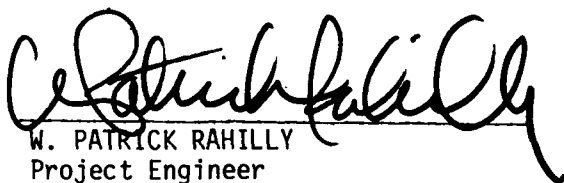
80 5 22 016

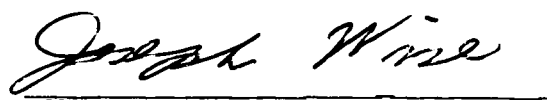
NOTICE

When Government drawings, specifications, or other data are used for any purpose other than in connection with a definitely related Government procurement operation, the United States Government thereby incurs no responsibility nor any obligation whatsoever; and the fact that the government may have formulated, furnished, or in any way supplied the said drawings, specifications, or other data, is not to be regarded by implication or otherwise as in any manner licensing the holder or any other person or corporation, or conveying any rights or permission to manufacture use, or sell any patented invention that may in any way be related thereto.

This report has been reviewed by the Office of Public Affairs (ASD/PA) and is releasable to the National Technical Information Service (NTIS). At NTIS, it will be available to the general public, including foreign nations.

This technical report has been reviewed and is approved for publication.

  
W. PATRICK RAHILLY  
Project Engineer  
Energy Conversion Branch  
FOR THE COMMANDER

  
JOSEPH F. WISE  
TAM, Solar Energy Conversion  
Energy Conversion Branch

  
JAMES D. REAMS  
Chief, Aerospace Power Division  
Aero Propulsion Laboratory

"If your address has changed, if you wish to be removed from our mailing list, or if the addressee is no longer employed by your organization please notify AFWAL/POOC-2, W-PAFB, OH 45433 to help us maintain a current mailing list".

Copies of this report should not be returned unless return is required by security considerations, contractual obligations, or notice on a specific document.

Unclassified

SECURITY CLASSIFICATION OF THIS PAGE (When Data Entered)

(9) REPORT DOCUMENTATION PAGE		READ INSTRUCTIONS BEFORE COMPLETING FORM
1. REPORT NUMBER (18) AFAPL-TR-79-2094	2. GOVT ACCESSION NO. AD-A084834	3. RECIPIENT'S CATALOG NUMBER
4. TITLE (and Subtitle) (6) RIBBON GROWTH OF SINGLE CRYSTAL GaAs FOR SOLAR CELL APPLICATION	5. TYPE OF REPORT & PERIOD COVERED Interim Technical Report Aug. 15, 1978-Aug. 15, 1979	6. PERFORMING ORG. REPORT NUMBER
7. AUTHOR(s) (10) Theresa A./Gould, Raymond G./Seidensticker, and Robert/Mazelsky	8. CONTRACT OR GRANT NUMBER(s) (15) Air Force Contract F33615-78-C-2031	
9. PERFORMING ORGANIZATION NAME AND ADDRESS Westinghouse Electric Corporation 1310 Beulah Road Pittsburgh, PA 15235	10. PROGRAM ELEMENT, PROJECT, TASK AREA & WORK UNIT NUMBERS (16) 3145 (17) 19/68 (13) 454	
11. CONTROLLING OFFICE NAME AND ADDRESS Air Force Aero Propulsion Laboratory/POE-2 Wright-Patterson AFB, OH 45433	12. REPORT DATE November 30, 1979	13. NUMBER OF PAGES 64
14. MONITORING AGENCY NAME & ADDRESS (if different from Controlling Office) DCASMA-Pittsburgh 1610-S. Federal Building 1000 Liberty Avenue Pittsburgh, PA 15222 (11) 30 Nov 77	15. SECURITY CLASS. (of this report) Unclassified	15a. DECLASSIFICATION DOWNGRADING SCHEDULE
16. DISTRIBUTION STATEMENT (of this Report)  Approved for public release, distribution unlimited. 376350		
17. DISTRIBUTION STATEMENT (of the abstract entered in Block 20, if different from Report) (9) Interim Rept. 15 Aug 78-15 Aug 79		
18. SUPPLEMENTARY NOTES		
19. KEY WORDS (Continue on reverse side if necessary and identify by block number)		
20. ABSTRACT (Continue on reverse side if necessary and identify by block number)  This report describes the first 12 months of a program to develop GaAs dendritic web. Liquid encapsulation with B2O3 is used to suppress As vaporization from the melt. Standard web growth system design and experimental techniques which have been developed at Westinghouse for Si web are also utilized for the GaAs program. Critical optimization of thermal geometry is achieved with computerized thermal modeling. (over)		

DD FORM 1 JAN 73 1473 EDITION OF 1 NOV 65 IS OBSOLETE

Unclassified 376350  
SECURITY CLASSIFICATION OF THIS PAGE (When Data Entered)

Unclassified

SECURITY CLASSIFICATION OF THIS PAGE(When Data Entered)

BLOCK 20 Abstract

→ Dendritic growth and web buttoning of GaAs have been observed in the current program. Web crystals have not yet been produced, however, a piece of primitive web material has been recovered from the system. The growth behavior and the morphology of GaAs dendrites, buttons, and web material are analagous to the results obtained from successful Si and Ge web growth systems. The thermal modeling results also indicate that the liquid encapsulated GaAs system is suitable for web growth.

+

Unclassified

SECURITY CLASSIFICATION OF THIS PAGE(When Data Entered)

# FOREWORD

This Technical Report covers all work performed under Contract No. F33615-78-C-2031, entitled "Ribbon Growth of Single Crystal GaAs for Solar Cell Application." The effort was sponsored by the Air Force Aero Propulsion Laboratory, Air Force Systems Command, Wright-Patterson Air Force Base, Ohio under Project 3145. Dr. W. Patrick Rahilly (AFAPL/POE-2) was the Air Force Project Engineer, while Theresa Gould of Westinghouse Electric Corporation was technically responsible for the work.

The authors wish to thank A. M. Stewart for his capable technical assistance throughout the program. The construction of the thermal model by E. Miksch is also acknowledged. Appreciation is extended to D. L. Barrett, C. S. Duncan, R. H. Hopkins, and T. R. Au Coin (U. S. Army Electronics Technology and Device Lab) for many helpful discussions.

APPROVAL FOR	
DATE	BY
100 PM	
DR. W. P. RAHILLY	
JAN 10 1979	
BY	
CHIEF OF	
AFAPL/POE-2	
DIST	AFAPL/POE-2
A	

# TABLE OF CONTENTS

SECTION	PAGE
I INTRODUCTION . . . . .	1
II PROGRAM PLAN . . . . .	6
III TECHNICAL STATUS . . . . .	9
3.1 Experimental System . . . . .	9
3.1.1 Growth Facilities. . . . .	9
3.1.2 Materials. . . . .	12
3.1.3 Lid Design . . . . .	13
3.2 Crystal Growth Results. . . . .	19
3.3 Encapsulant Behavior. . . . .	33
3.4 Thermal Modeling. . . . .	36
3.4.1 Heat Flow Analysis . . . . .	36
3.4.2 Refraction Analysis. . . . .	38
3.4.3 Modeling Results . . . . .	38
3.5 Projected System Refinements. . . . .	46
3.5.1 Temperature Stability. . . . .	46
3.5.2 Stress Reduction . . . . .	47
3.5.3 System Flexibility . . . . .	47
IV CONCLUSIONS. . . . .	48
APPENDIX A Standard Operating Procedures. . . . .	49
APPENDIX B Analytical Treatment of Radiant Heat Transfer. . . . .	52
REFERENCES . . . . .	55

## LIST OF ILLUSTRATIONS

FIGURE	PAGE
1 Schematic Section of Web Growth. . . . .	2
2 Temperature Dependence of the Dissociation Pressure of GaAs. <sup>(2)</sup> At Standard Atmospheric Pressure As is Lost During Melting Unless Measures are Taken to Retain it . . . . .	4
3 Schematic of the Liquid Encapsulation Technique. . . . .	5
4 The Modified A. D. Little Crystal Growing Furnace. . . . .	10
5 Web Growth Susceptor Assembly. . . . .	11
6 Schematic Section of Web Compared with the Temperature Profile at the Melt Surface. . . . .	14
7 Temperature Profile in the Melt Produced by a Dogbone Slot, D, and a Straight Slot, S. The Flattened Profile Produced by the Dogbone Slot is Well Suited for Web Growth. . . . .	15
8a Lid #1 - The First Slot Design Used for GaAs Dendrite Growth Runs . . . . .	17
8b Lid #1 mod- Modification of Lid #1 Produced a Successful Design for Dendrite Growth . . . . .	17
9a Lid #2-Buttoning Behavior was Greatly Improved with an Elongated Slot . . . . .	18
9b Lid #3 - A Wide Dogbone Slot was Used in the Thermal Model and is Currently in Use in the Growth System . . . . .	18
10 GaAs Dendrite after B <sub>2</sub> O <sub>3</sub> Removal . . . . .	21
11 Typical Dendrite Surface at 100X . . . . .	22
12 Dendrite Cross Section Revealing Degenerate Twin Structure. 100X . . . . .	23
13 Non-Degenerate Twin Shown at 100X. . . . .	24
14 Degenerate Twin Structure of a Three Twin Dendrite. 500X .	25

# LIST OF ILLUSTRATIONS

FIGURE		PAGE
15	Morphology of the GaAs Button (Top) is Similar to the S <sup>4</sup> Button Shown Below it. . . . .	28
16	Cross Section Taken Through the Top of the GaAs Button Shown in Figure 15. 100X. . . . .	29
17	Cross Section Taken Through the Side of the GaAs Button and the Penetrating Dendrite. 100X. . . . .	30
18	A Segment of GaAs Web Material. The Flat Morphology Contrasts with the Thick, Choppy Dendrite Bordering the Left Side. . . . .	31
19	Cross Section of the Web Material Shown in Figure 18. A Wide Twin and a Second Very Narrow Twin are Visible Near the Top of the Sample. 100X . . . . .	32
20	For the Upper Figure the Viewfactors from Points on the Melt Surface can be Calculated Analytically. The Presence of a Refracting Layer (Lower Figure) Changes the Path of the Radiation and Alters the Viewfactors to the Slot . . . . .	37
21	Schematic Diagram of the Logic of the Ray-Tracing Program. Radiation from the Melt Surface Strikes the Lower Susceptor Wall or the B <sub>2</sub> O <sub>3</sub> Surface. Rays Striking the B <sub>2</sub> O <sub>3</sub> Surface are Reflected or Refracted. Reflected Rays Undergo Total Internal Reflection Until they Strike the Lower Wall. Refracted Rays Strike the Upper Wall, the Lid, or Exit Through the Slot . . . . .	39
22	Heat Loss Through the Slot from Points on the GaAs Surface which Lie Under the Long Axis of the Slot. Increasing Depths of B <sub>2</sub> O <sub>3</sub> Increase the Radiative Loss through the Slot . . .	40
23	Heat Loss Through the Slot from Points on the GaAs Surface which Lie Perpendicular to the Slot. . . . .	41
24	Isotherms Generated by the WECAN Model for One Quadrant of the GaAs Melt Surface. . . . .	43
25	WECAN Thermal Cross Section of the Melt Parallel to the Long Axis of the Slot. Inversion of the Isotherms Occurs in the B <sub>2</sub> O <sub>3</sub> . . . . .	44
26	WECAN Thermal Cross Section of the Melt Perpendicular to the Long Axis of the Slot. . . . .	45

# LIST OF TABLES

TABLE		PAGE
1	Program Schedule. . . . .	8
2	Crystal Growth Results. . . . .	20
3	Buttoning Summary . . . . .	27
4	Composition Analysis of Used Melts. . . . .	34
5	Etchants for GaAs . . . . .	51

## SECTION I

### INTRODUCTION

This report describes the first twelve months (Phase I) of a 3-year program to develop GaAs dendritic web for high efficiency solar cells. The work reported was performed from July, 1978, through July, 1979.

The overall goal of the program is to demonstrate the utility of the dendritic web process for the economical production of GaAs substrate material. The major thrust of Phase I has been an assessment of the feasibility of liquid encapsulated GaAs dendritic web growth. Although the production of high quality GaAs web crystals has been impeded by experimental difficulties, the growth of primitive web material has been successfully demonstrated. The problems encountered in Phase I have been mechanical or systematic and no limitation of a fundamental nature which would preclude GaAs web growth has been encountered. The Phase I experimental and analytical results confirm the feasibility of the liquid encapsulated dendritic web technique for the growth of GaAs.

Dendritic web morphology is shown schematically in Figure 1. A seed dendrite with the required twin plane structure is brought into contact with the melt at the "hold" temperature. At this temperature the seed neither melts nor nucleates growth. As the melt is undercooled, the twin structure of the seed and the attachment kinetics associated with the thermal environment induce the growth of a lateral "button." When the button is pulled from the melt, two dendrites propagate from the ends and a film of liquid is drawn up between them. This film freezes into a smooth ribbon with a single crystal surface well suited for subsequent device fabrications. The dendritic web technique has been highly successful for the growth of both Si and Ge crystals.

Dwg. 6256A82

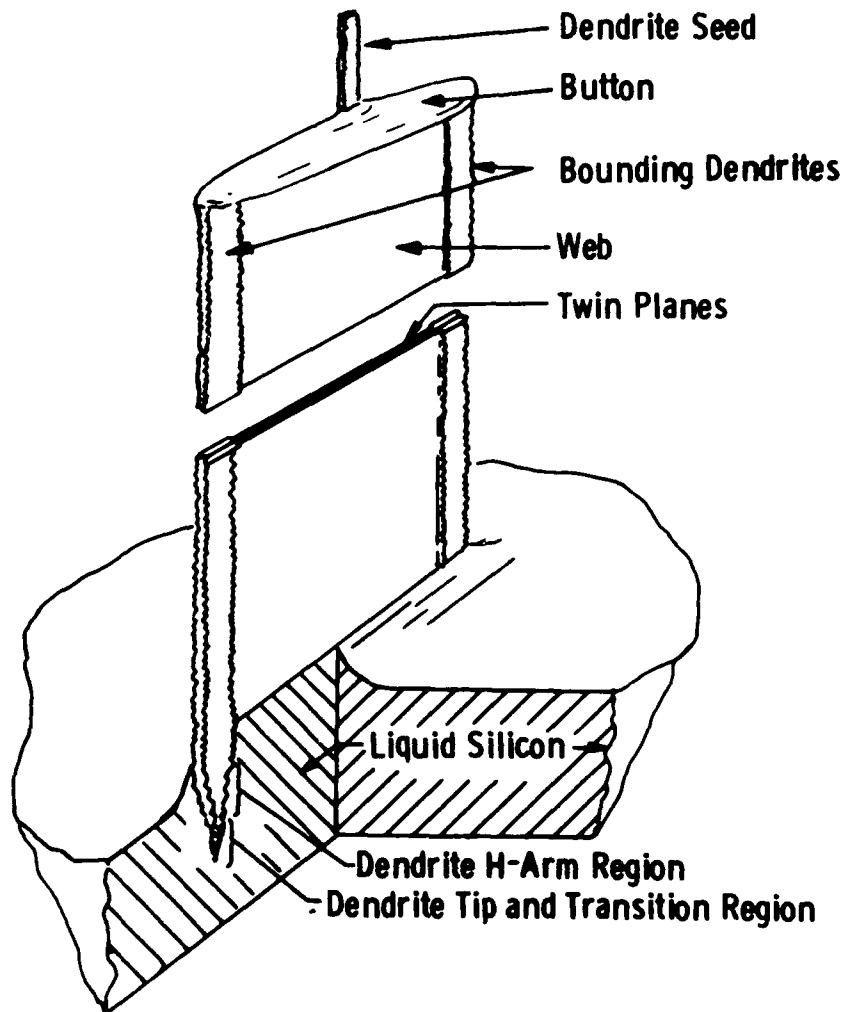


Fig. 1 - Schematic section of web growth

Dendritic morphology in GaAs was demonstrated at Westinghouse in 1964 under a prior Air Force contract.<sup>(1)</sup> High quality dendritic material was not obtained due to inadequate control of As vaporization and the resultant composition changes. (See Figure 2).

The liquid encapsulation technique is a unique approach to dissociation control of volatile compounds.<sup>(3)</sup> The prior method required a controlled As atmosphere over the melt and necessitated a complex furnace design. In the liquid encapsulation method the stoichiometry is controlled by covering the melt with an inert liquid, usually  $B_2O_3$ . A bucking pressure in excess of the vapor pressure of the volatile constituent is maintained over the melt. (Figure 3). Liquid encapsulation with  $B_2O_3$  has become widely used for Czochralski growth of GaAs<sup>(4-9)</sup> and was adopted for the current dendritic web growth program.

At the inception of the current program the effect of the  $B_2O_3$  layer on the growth of web was a matter of concern. The effect of the encapsulant on the ability to undercool the melt was unknown.  $B_2O_3$  is a getter of foreign oxides thereby introducing the possibility of spontaneous nucleation at the undercooled  $B_2O_3$ -GaAs interface. The visibility through the encapsulant which is required for controlled seeding on a dendrite, buttoning, and growth was not demonstrated. The thermal effects of a refracting layer covering the melt were unknown. The experimental results of Phase I, however, have demonstrated that  $B_2O_3$  encapsulation is compatible with the growth procedures that are required for dendritic web.

In addition to the stoichiometry problem described above, the experiments conducted under the prior GaAs web growth contract were impeded by insufficient optimization of the thermal geometry. Thermal variables in a web growth system interact in a complex fashion and the exact conditions that are critical to successful web growth are difficult to predict on a completely empirical basis. A thermal modeling approach developed at Westinghouse for Si web has been highly useful for systematic optimization. Therefore, an existing computer heat flow analysis has been adapted for use with the liquid encapsulated GaAs system. The initial thermal analysis performed during Phase I indicates that the system is thermally suitable for dendritic web growth.

Curve 718160-A

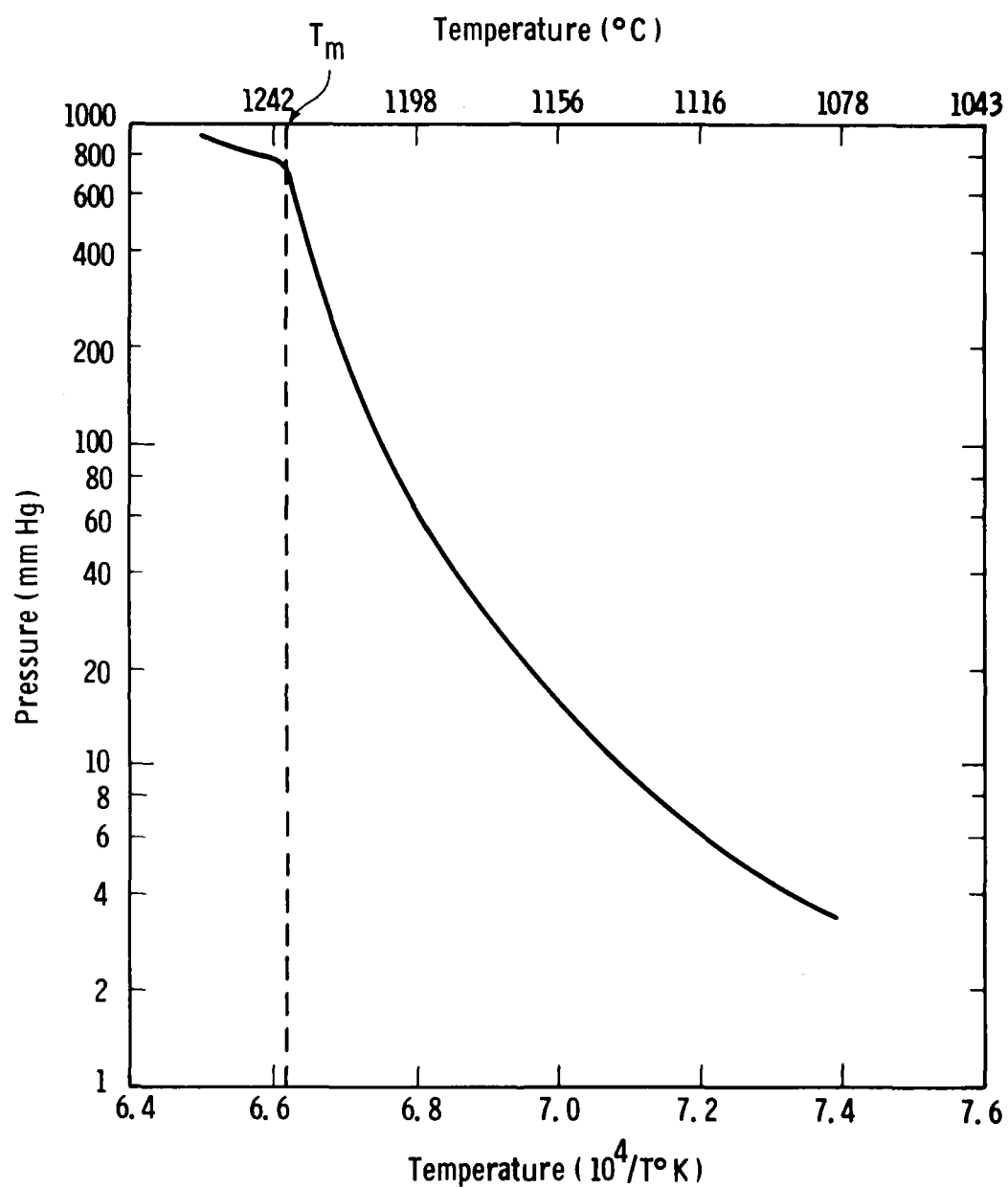


Figure 2 Temperature Dependence of the Dissociation Pressure of GaAs. (2) At Standard Atmospheric Pressure As is Lost During Melting Unless Measures are Taken to Retain it.

Dwg. 7702A27

Inert Gas Pressure > 1 Atm.

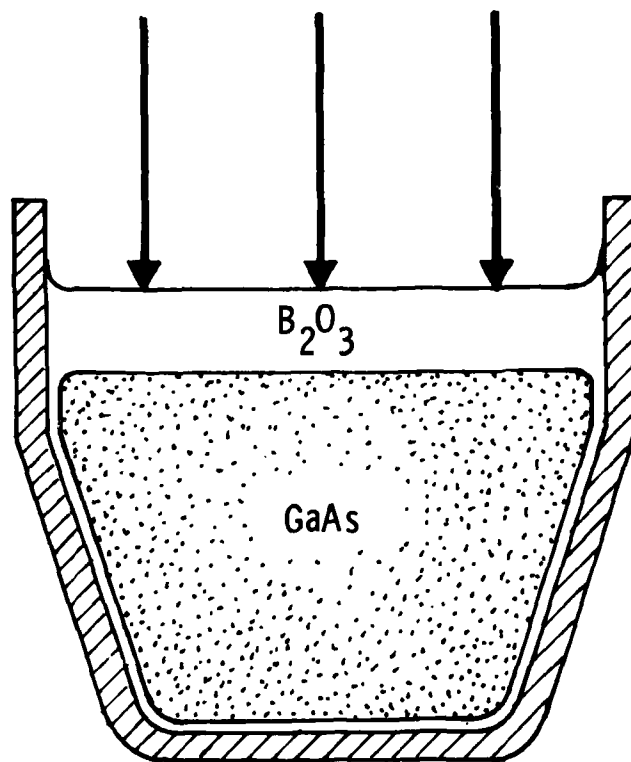


Figure 3 Schematic of the Liquid Encapsulation Technique

## SECTION II

### PROGRAM PLAN

In order to meet the objectives of this program background in thermal modeling, crystal growth theory, and practical crystal growth experience will be utilized systematically to progress toward the demonstration of GaAs web growth. Thermal models tested and refined by experiment will be the basic guide for verification of the parameters required for growth of web. These will provide first order susceptor, crucible, lid configurations from which initial growth will be attempted. Iteration of experimental data and computer models will continue until a satisfactory design for web growth is established. During Phase II of the program the furnace will be scaled upwards to permit larger widths of web and the growth of n-type GaAs web will be demonstrated.

The elements which comprise the program plan include thermal modeling, model verification, dendritic growth, and web growth.

The thermal modeling will be based on the crucible/furnace configuration designed to accommodate the growth of 1.2 cm wide web. This will require a crucible diameter of 4-5 cm. Past experience has shown that the most desirable design is somewhat dish shaped rather than cylindrical and a computer program for this configuration already exists. It is anticipated that the height of the crucible will be approximately 3 cm and a crucible load will be approximately 100 grams of gallium arsenide. The preliminary design of the crucible/susceptor/shields/lid will be modeled and vertical and horizontal temperature gradients will be calculated using the WECAN finite element code. (Because of the potential impact of light piping in the  $B_2O_3$  layer on the temperature distribution in the GaAs melt, the model was extended to include ray tracing).

Model verification will be performed by temperature measurements in the melt and the susceptor using both a model material and GaAs itself. As a final step in the verification procedure GaAs- $B_2O_3$  will be melted in the furnace and dendrite probes at the surface of the melt will

be performed. This will verify that a dendrite can be maintained in contact with the GaAs melt through the  $B_2O_3$  encapsulant. Positioning the dendrite probe along the slot will also serve to verify the extent of the isothermal region at the surface of the melt.

Dendrites are required as seeds for web growth. The most convenient source of dendrites is the rapid insertion and withdrawal of a polycrystalline seed into an undercooled melt. Small dendrites having appropriate twin spacings can be selected. These will be used as seeds from which longer dendrites can be grown which can then be cut to length for seeding web growth.

The initiation of web growth requires controlled formation of a button and subsequent dendrite formation at the end of the button. Upon withdrawal of the button the bounding dendrites are required to penetrate into the melt and allow the formation of the molten web between them. Buttoning and the formation of bounding dendrites are primarily a function of undercooling and the temperature gradients, both transverse and vertical. Developing the correct conditions requires a systematic study of the effects of degree of undercooling and controlled temperature gradients. Observation of the web during growth will be the prime determinant in the deformation of growth parameters.

During this phase of the program analysis will be primarily confined to structural techniques such as etching, microscopy and x-ray analysis. Resistivity and Hall measurements will be performed on selected samples as appropriate.

TABLE 1  
PROGRAM SCHEDULE

TASK	2	4	6	8	10	12	14	16	18	20	22	24	26	28	30	32	34	36
1. Model Development	Δ				Δ	Δ	Δ	Δ										
2. Model Verification		Δ																
3. Dendrite Growth			Δ															
4. Web Growth				Δ														
5. Analysis o GaAs o System						Δ	Δ	Δ										
6. Phase I Tech. Rpt.							Δ											
7. Sample Delivery							Δ											
8. Apparatus Mod						Δ												
9. n-type Doping Study							Δ											
10. Model Refinement							Δ					Δ						
11. Web Growth								Δ										
12. Material Diagnostic									Δ									
13. Web Analysis														Δ				
14. System Analysis															Δ			
15. Sample Delivery																		
16. Final Report																	Δ	Δ

## SECTION III

### TECHNICAL STATUS

#### 3.1 EXPERIMENTAL SYSTEM

##### 3.1.1 Growth Facilities

An A. D. Little crystal growing furnace has been used throughout the program for the growth of material. The overpressures that are required for liquid encapsulated growth are well within the limits of the apparatus and slight modification of the standard MP model produced an adequate web growth facility.

The major features of the modified system are shown in Figure 4. The molybdenum susceptor is heated by induction at a frequency of 10 kHz. Thermocouples used for sensing susceptor temperatures are introduced through the bottom seal. An automatic temperature control system utilizes light pipe output from the outer wall of the susceptor. A radiamatic sensing unit and an Azar L&N controller maintain temperatures to within  $\pm 1^\circ\text{C}$ . The susceptor assembly is designed to provide vertical positioning via a threaded turning ring (not shown). Therefore, the vertical temperature gradient in the melt can be adjusted by moving the susceptor with respect to the coil.

The susceptor assembly is shown in greater detail in Figure 5. Heat loss from the bottom of the susceptor is minimized by radiation shields and insulating support pins in the tripod mount (only one leg of the tripod is shown). The thermal conditions required for web growth are imposed on the melt by the slotted lid and top shield. The slot shape that is shown is a standard web lid design adopted from Si web experience.

The axial thermocouple penetration is shown in Figure 5. Four symmetrically arranged peripheral positions are also provided in the susceptor. Originally Inconel sheathed Type B thermocouples obtained from Marlin Manufacturing Corporation were used in all five positions. At the required operating temperatures, however, the sheath of the

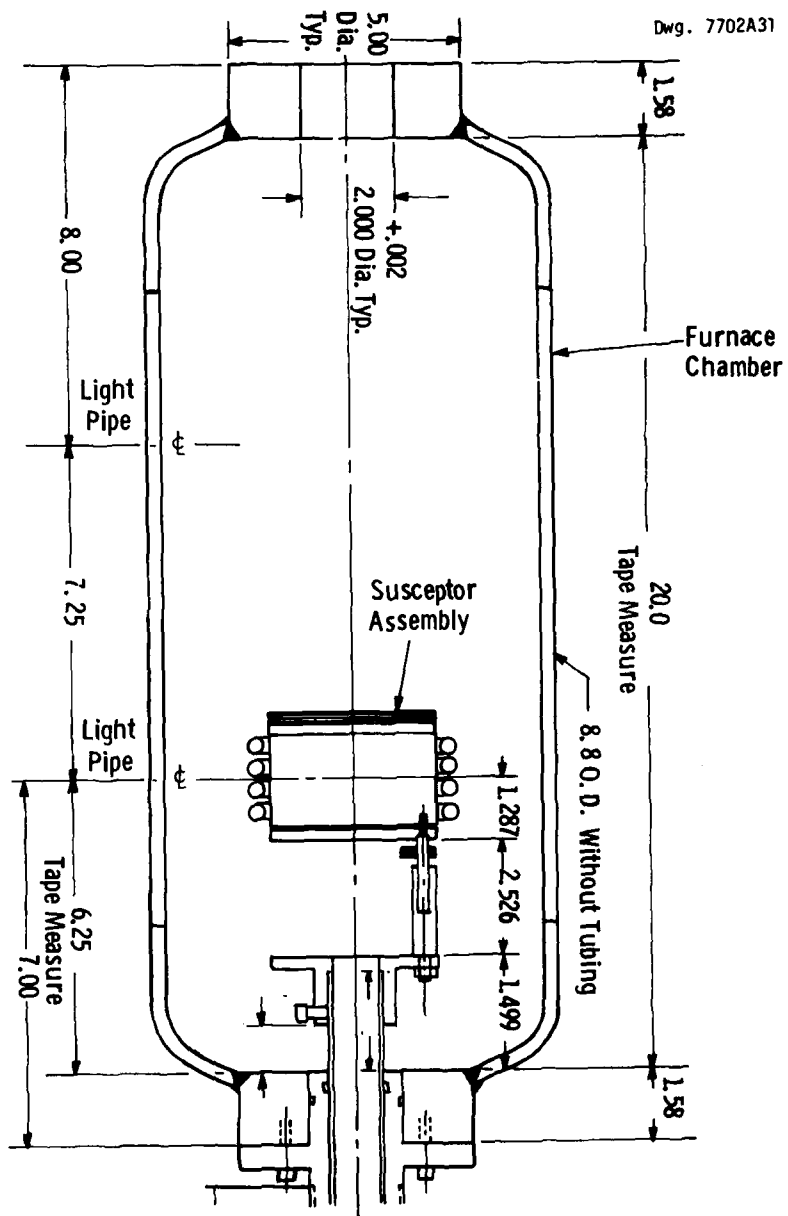


Figure 4 The Modified A.D. Little Crystal Growing Furnace

Dwg. 7702A28

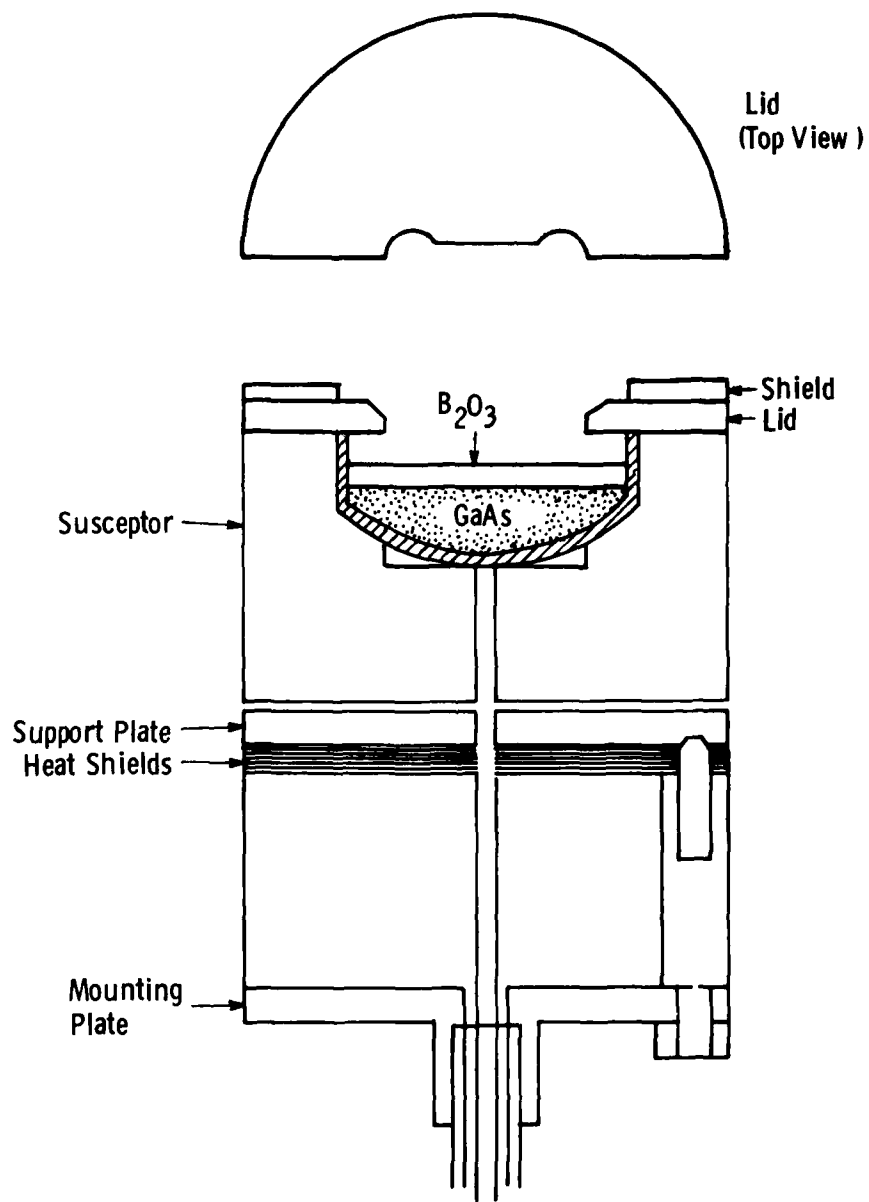


Figure 5

Web Growth Susceptor Assembly

thermocouples reacted rapidly with the molybdenum susceptor. Thermocouples of this type protected from the susceptor with an alumina cap provided only marginal improvements in thermocouple life. A molybdenum sheathed Type B thermocouple is currently in use in the axial position. The molybdenum sheath is too inflexible, however, to withstand the bending that is required to position a peripheral thermocouple.

Crucibles of fused quartz approximately two inches in diameter are used in the system. They are etched by the  $B_2O_3$  but not severely attacked. The  $B_2O_3$  also wets quartz which causes the crucibles to shatter on cooldown due to differential thermal expansion. However, this wetting behavior insures true encapsulation of the charge of GaAs by the  $B_2O_3$ .

The spherical shape of the crucibles illustrated in Figure 5 was adopted from Si web experience and is well suited for heat flow analysis with existing computer programs. A portion of the susceptor below the crucible is cut away to minimize thermal inconsistencies introduced by crucible variation. The provision of a sufficient gap under the crucible insures that all heat transfer in this region occurs by radiation and gas conduction for each crucible that is used. It has been discovered recently, however, that a different thermal stability problem may have been incurred by this design and revision of the susceptor design is planned (See Section 3.5).

Boric oxide is hygroscopic and therefore must be heated in vacuum prior to use as an encapsulant to avoid excessive bubbling resulting from the evolution of water vapor. A small drying furnace was assembled utilizing r-f heating coupled to a Pt-Au crucible. A quartz tube encloses the crucible and seals into a baseplate that provides controlled evacuation capability.

### 3.1.2 Materials

The  $B_2O_3$  which has been used routinely was obtained from Atomergic Chemetals Corporation. This high purity material is specifically designated as  $B_2O_3$  for liquid encapsulation. Ultra pure  $B_2O_3$  from

Alpha Inorganics and reagent grade  $B_2O_3$  from Fisher have also been used on occasion with no indications of significant differences in the melt appearance.

Semiconductor grade GaAs (five 9's purity) obtained from Morgan Semiconductor was used throughout much of Phase I. Both polycrystalline and single crystal material were used successfully. GaAs obtained from D. L. Barrett at the Westinghouse R&D Center has also been used. This material was reacted from starting components of six 9's purity obtained from Alusuisse, Cominco, or Johnson Matthey. Again no significant differences were observed with variation of material.

Since no GaAs dendrites were available for seeds, single crystal slivers fractured from GaAs wafers were used for most of the experiments. This technique produces much random dendritic propagation in unsuitable directions. During the second half of Phase I oriented seeding was attempted by using [211] seeds fractured from (111) wafers obtained from Morgan Semiconductor. No obvious improvement in the control of propagation directions was observed.

### 3.1.3 Lid Design

Details of the lid and slot design are critical for successful web growth. Heat flow analysis has shown that the thermal profile in the melt is largely determined by the slot geometry. Due to difficulties in obtaining programmer time, thermal modeling of the GaAs system was not completed until near the end of Phase I. Therefore, lid and slot geometries were designed on the basis of Si web experience and observation of the growth behavior.

The thermal profile at the surface of the melt must be flat over an adequate distance for successful web growth. This provides uniform growth conditions for a web crystal of the desired width as shown in Figure 6. Thermal modeling of Si web systems has shown that a slot having open end holes flattens the temperature profile in the melt in the manner illustrated in Figure 7. Therefore, "dogbone" slot designs are routinely used for web growth.

Dwg. 6438A24

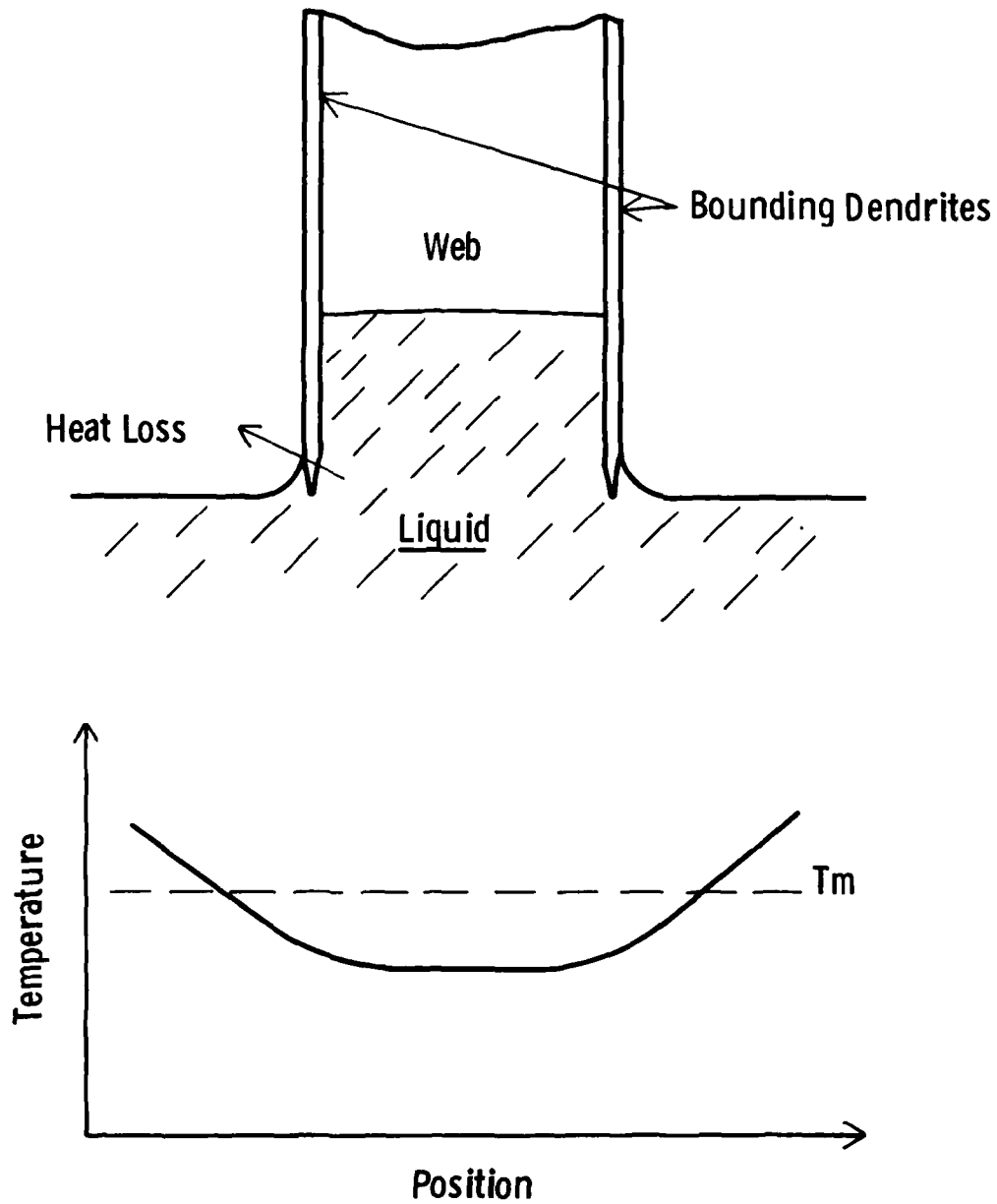


Figure 6 Schematic Section of Web Compared with the Temperature Profile at the Melt Surface.

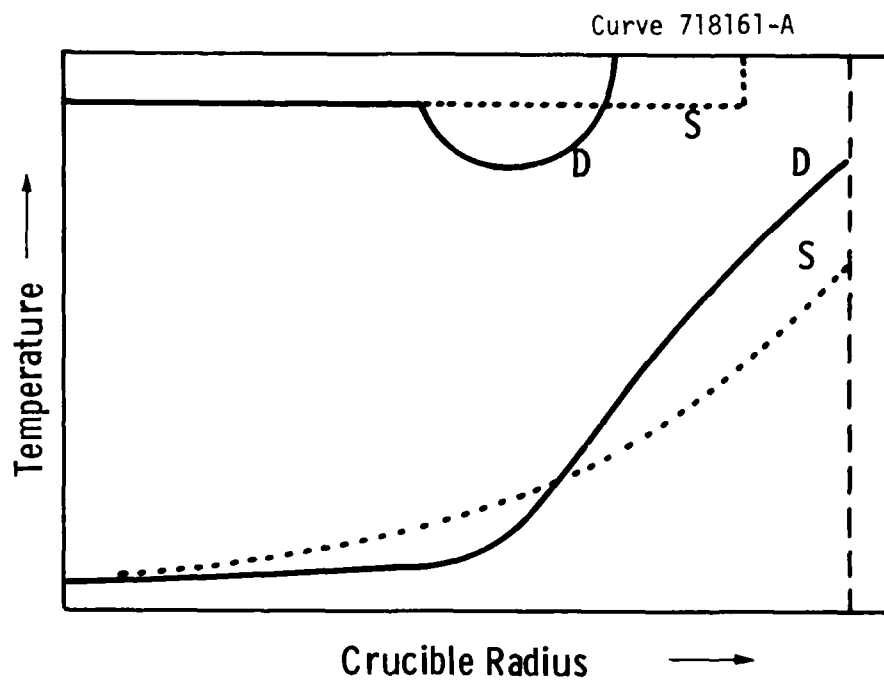


Figure 7 Temperature Profile in the Melt Produced by a Dogbone Slot, D, and a Straight Slot, S. The Flattened Profile Produced by the Dogbone Slot is Well Suited for Web Growth.

The first lid used in the GaAs system was a conventional dogbone design with the dimensions given in Figure 8a. Initial dendrite growth attempts were hampered by this design, however. Randomly branching dendritic growth could not be pulled past the lid, and the high temperature in the narrow slot appeared to cause As loss from the seeds.

In order to correct the problems associated with dendritic growth from Lid #1, a large hole was introduced into the slot (See Figure 8b). The lid was no longer useable as a web lid. However, the growth of seed-type dendrites was achieved immediately following this modification.

Although primitive buttoning was observed with the modified Lid #1, a web type lid was required to adequately evaluate the buttoning phenomenon. Lid #2 (Figure 9a) was designed with a wide straight slot. The effect of this slot change on the buttoning behavior of the system was dramatic (See Table 3, Section 3.2) and many web type buttons were grown using this lid.

The thermal analysis of the system was performed for the wide dogbone slot shown in Figure 9b. This lid was subsequently fabricated and is currently in use to provide a comparison of experimental and analytical results.

Dwg. 7702A30

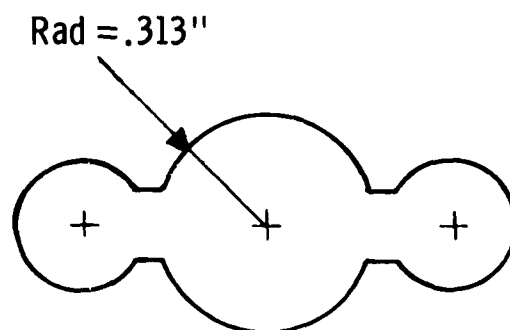
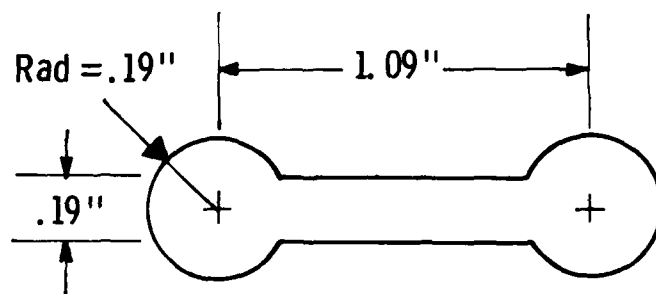


Figure 8b. Lid # 1mod - Modification of Lid #1 Produced a Successful Design for Dendrite Growth.

Dwg. 7702A29

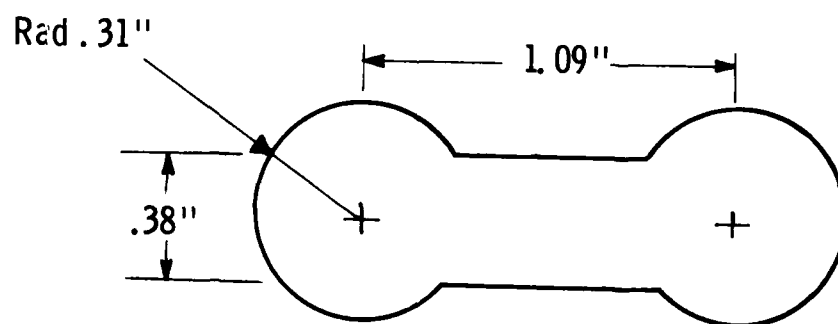
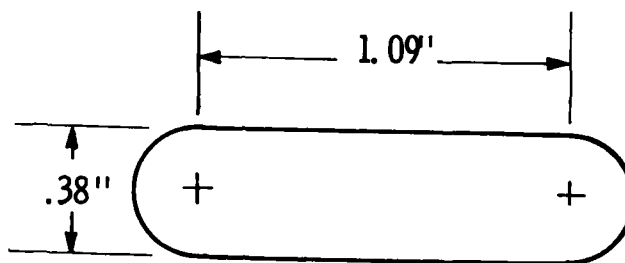


Figure 9b. Lid #3 - A wide Dogbone Slot was Used in the Thermal Model and is Currently in Use in the Growth System.

### 3.2 CRYSTAL GROWTH RESULTS

GaAs dendrites, buttons, and web material have been grown from the liquid encapsulated system. A summary of material data is given in Table 2.

A total of 25 growth runs were made during Phase I, and at least one dendrite was grown in each run. Due to further experimentation or material breakage only 13 of 42 dendrites have been recovered for characterization.

Typical GaAs dendrite morphology is illustrated in Figures 10 and 11. The well-faceted structure shown in Figure 11 is characteristic of dendritic growth seen in Si and Ge. The dark feature in the center of the dendrite face has the appearance of frozen liquid. Trapping of liquid droplets in this region has been observed in Ge dendrites and is well explained by dendritic growth theory.<sup>(10)</sup>

The surface of most of the dendrites exhibit other small droplet like marks such as those shown in the upper half of Figure 11. These features have the appearance of inclusions. No detailed composition analysis of grown material has been performed during Phase I. However a typical inclusion-like structure on a particular dendrite was examined with electron dispersive analysis. The composition of the entire droplet feature was GaAs with some Ga enrichment in specific areas. No free Ga was detected. Therefore, we conclude that there is no excessive As loss from growing material and further improvement in composition is expected as the thermal design is optimized.

The twin structure and spacing in the dendrites is also analagous to that seen in Si and Ge. Most of the dendrites contain two twin planes that are degenerate, i.e. do not continue to the edge of the dendrite (Figure 12). A few of the twins are non-degenerate (Figure 13) and two of the dendrites contain three twin planes as shown in Figure 14. Dendritic propagation is not perturbed by twin degeneration, however, it may be detrimental to seeding and buttoning.<sup>(11)</sup>

TABLE 2

## CRYSTAL GROWTH RESULTS

MATERIAL	STATISTICS		GROWTH HABIT	TWIN STRUCTURE	
	Number Grown	Number Recovered		Number of Twin Planes	Twin Plane Spacing
DENDRITES	42	13	Degenerate Twins - 10 Non-degenerate Twins - 4*	Two twin planes - 11 (85%) Three twin planes - 2	.72 $\mu$ - 7.82 $\mu$
BUTTONS	37	2	Polycrystalline - 4 Hexagonal - 7 Elongated - 26 (70%)	Hexagonal Button - no twin Web Button - 3	.81 $\mu$ & 56.3 $\mu$
WEB MATERIAL	1	1	-	3 Twin planes present	1.55 $\mu$ & 55 $\mu$

\* In one dendrite the twin structure was non-degenerate in one segment that was characterized and degenerate in a different portion.

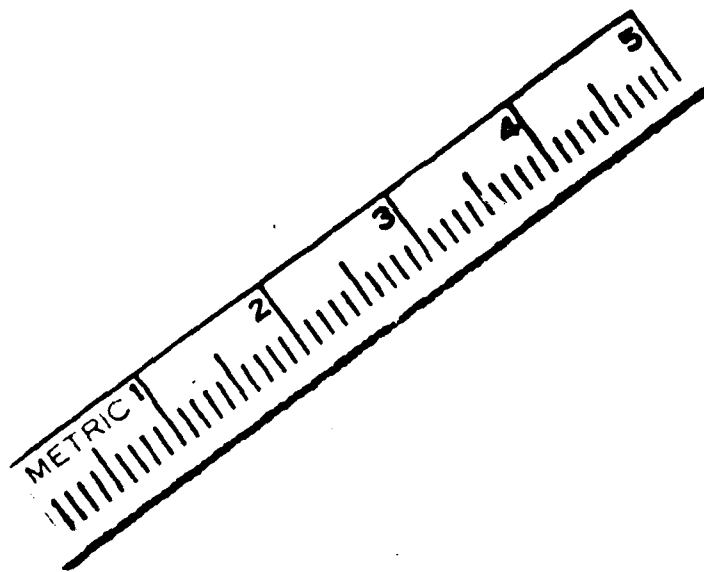


Figure 10 GaAs Dendrite after B<sub>2</sub>O<sub>3</sub> Removal.



Figure 11 Typical Dendrite Surface at 100X.

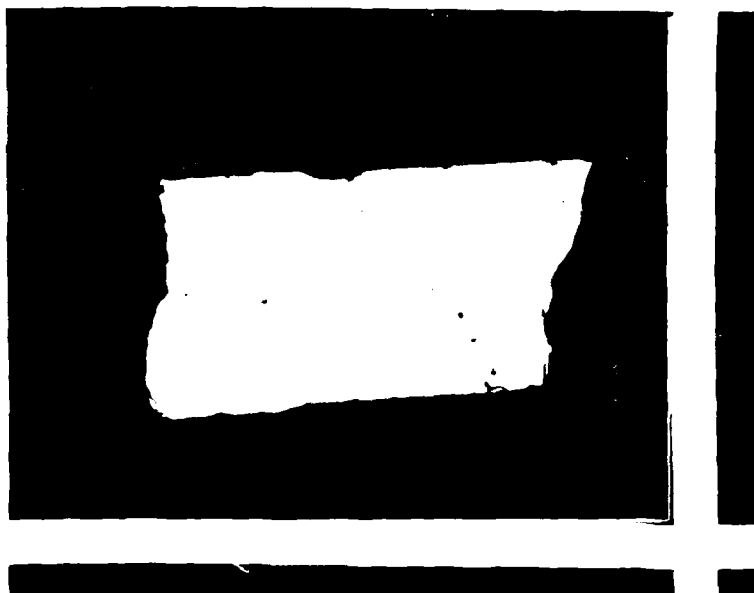


Figure 12 Dendrite Cross Section Revealing Degenerate  
Twin Structure. 100X.



Figure 13 Non-Degenerate Twin Shown at 100X.



Figure 14      Degenerate Twin Structure of a Three Twin Dendrite.  
500X.

The buttoning behavior which has been observed for GaAs is similar to Si web buttoning. As Table 2 indicates, the overwhelming majority of GaAs buttons that have been grown are of the elongated web type.

The effect of lid design on buttoning is illustrated in Table 3. Establishment of a web growth thermal profile in the melt with lid #2 greatly increased the percentage of web buttons that were produced. (Hexagonal buttons result from the (111) orientation when the twin structure of the seed is not propagated through the button. If the nucleated growth is not oriented by the seed dendrite a shapeless polycrystal results.)

The most striking example of web button morphology that has been observed for GaAs is shown in Figure 15. A Si web button is given for comparison. The lack of web between the side dendrites is symptomatic of an incorrect pull speed/undercooling relationship in both cases. The twin structure across the top of the GaAs button and through the side dendrite is shown in Figures 16 and 17. A very wide twin is evident and it appears that a third twin plane with an extremely small spacing is also present.

A section of a piece of web material which has been recovered from the system is shown in Figure 18. Uncontrolled dendritic propagation precluded the growth of a good web crystal. However, the material does exhibit a flat, web-like morphology. Microscopic examination of a cross-section of this material reveals three twin planes (Figure 19), thereby confirming its web character.

TABLE 3

## BUTTONING SUMMARY

LID #1 Mod.

NUMBER OF BUTTONS	-	7	
POLYCRYSTALLINE	-	4	
HEXAGONAL	-	2	
ELONGATED	-	1	(14%)

LID #2

NUMBER OF BUTTONS	-	30	
POLYCRYSTALLINE	-	2	
HEXAGONAL	-	3	
ELONGATED	-	25	(83%)

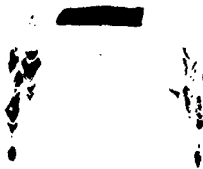
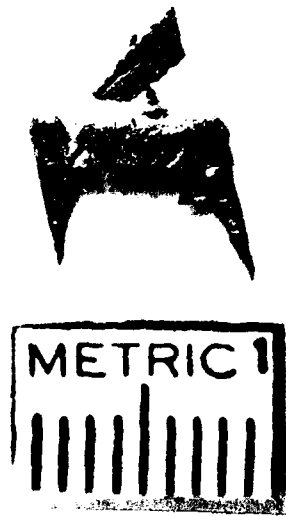


Figure 15. Morphology of the GaAs Button (Top) is Similar to the Si Button Shown Below it.



Figure 16 Cross Section Taken Through the Top of the GaAs Button Shown in Figure 15. 100X.

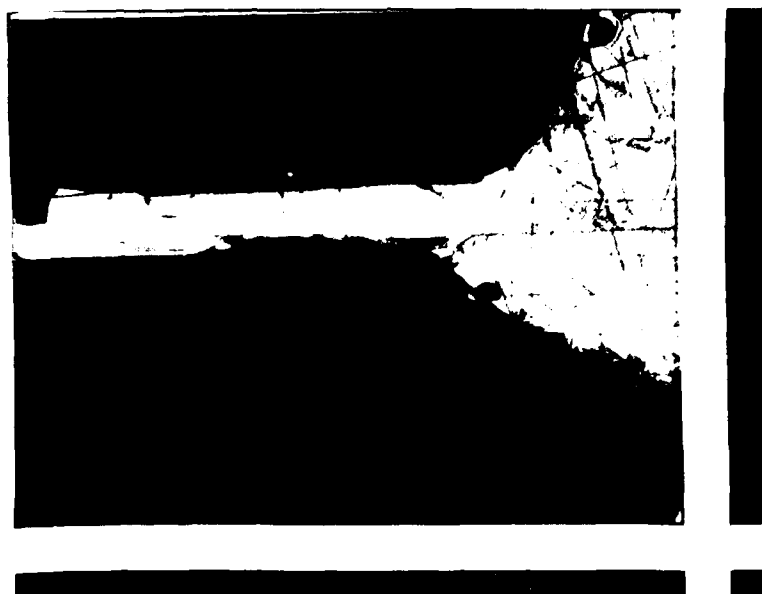


Figure 17 Cross-Section Taken Through the Side of the GaAs Button and the Penetrating Dendrite. 100X.

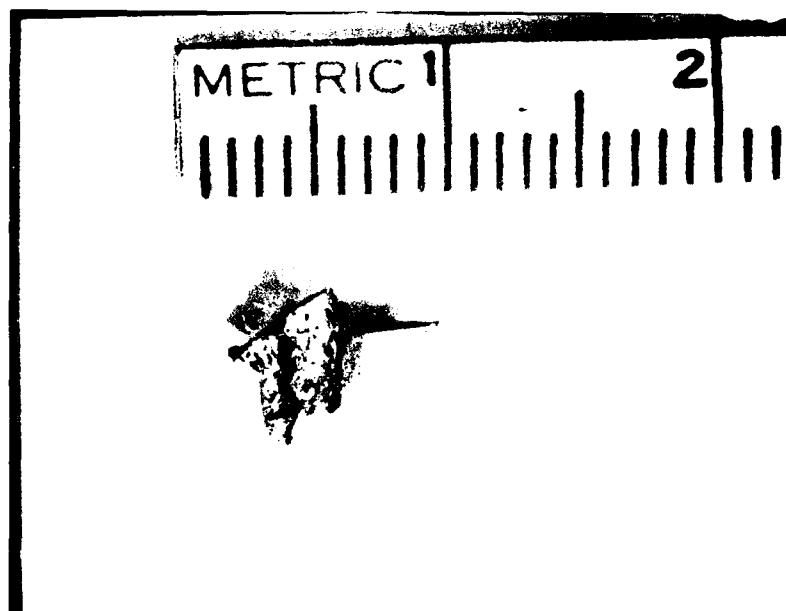


Figure 18      A Segment of GaAs Web Material. The Flat Morphology Contrasts with the Thick, Choppy Dendrite Bordering the Left Side.

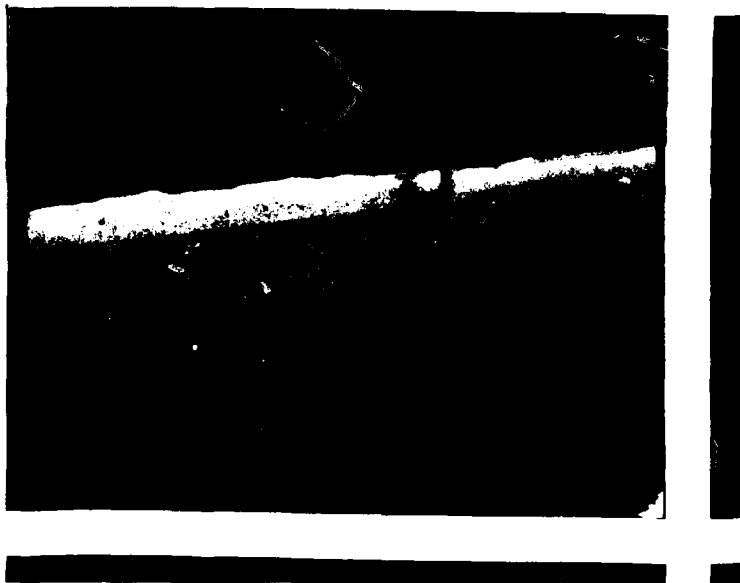


Figure 19 Cross Section of the Web Material Shown in Figure 18.  
A Wide Twin and a Second Very Narrow Twin are Visible  
Near the Top of the Sample. 100X.

### 3.3 ENCAPSULENT BEHAVIOR

The use of  $B_2O_3$  as the encapsulent for the GaAs web growth system has been satisfactory. Visibility is adequate for determination of hold and buttoning. The presence of the encapsulent does not interfere with the nucleation and growth of material from the melt surface. The gettering action of the  $B_2O_3$  appears to be compatible with web growth procedures.

The  $B_2O_3$  wets the quartz crucible thereby truly encapsulating the melt. The stoichiometry of the melt is adequately maintained by a 5-6 mm layer of  $B_2O_3$ . The results of a chemical analysis of several used melt samples are given in Table 4. These samples were taken from early experiments in which melt down vaporization was not totally controlled. Even under this unfavorable condition, the composition of the melt was not greatly disturbed.

After use the cooled  $B_2O_3$  is gray and opaque. It has been found that the presence of both Ga and Si is necessary to produce this discoloration. It is evident that the  $B_2O_3$  etches the quartz crucible thereby dissolving  $SiO_2$ . Experimentation with liquid encapsulated Czochralski systems indicate that gallium oxide is dissolved in the  $B_2O_3$  due to the presence of residual water.<sup>(6,7)</sup> This slight reactivity of the  $B_2O_3$  with the melt and crucible does not appear to impair crystal growth.

The  $B_2O_3$  is usually picked up by growing GaAs in isolated droplets which rapidly freeze on the surface as the material is pulled above the lid. Some stress is induced in the material due to uneven distribution of the  $B_2O_3$  which is caused by thermal asymmetry. Material breakage on cool down has been reduced by releasing the pressure in the system once the susceptor has reached 800°C.

Material stress also occurs when the  $B_2O_3$  is rehydrated by exposure to the atmosphere, or in the process of dissolution in water. Less material breakage is incurred by removal of  $B_2O_3$  with concentrated HF.

TABLE 4

COMPOSITION ANALYSIS OF USED MELTS

<u>Run</u>	<u>Ga-wt.% (<math>\pm 0.25\%</math>)</u>	<u>As-wt.% (<math>\pm 1.0\%</math>)</u>
6	48.14	51.40
7	48.32	51.12
8	48.53	51.34
9	48.47	51.30
10	48.30	50.44
11	48.04	51.38

STOICHIOMETRIC COMPOSITION (wt.%)

Ga - 48.2%

As - 51.8%

The presence of the encapsulant at the melt surface modifies the thermal characteristics of the system. The  $B_2O_3$  is essentially transparent;<sup>(12)</sup> however, refraction in the layer alters the radiation exchange between the melt surface and its environment. Both experimental observations and modeling results indicate that the  $B_2O_3$  surface is slightly warmer than the GaAs surface for conventional web lid designs. This effect can be controlled by adjustment of the thermal geometry and is not expected to impair web growth.

### 3.4 THERMAL MODELING

#### 3.4.1 Heat Flow Analysis

Web growth systems characteristically involve many interrelated thermal variables which are critically dependent on small changes in the thermal geometry. It is difficult to predict the effect of a given modification on a purely empirical basis. Therefore, analytical methods are necessary for the optimization of growth conditions. The utility of a computerized thermal model has been demonstrated in the Si web program, and the same modeling approach was adopted for GaAs web.

The thermal model evaluates the temperature distribution in the susceptor/crucible/melt system for given input conditions. A finite element technique is utilized to perform a steady state heat flow analysis. The statement and solution of the problem is performed with WECAN, a proprietary analytical code. The flexibility of this code permits great freedom for modification of the system geometry in the model. Thus, small changes in the system can be faithfully modeled with little effort once the original set of elements has been established.

The analysis treats conductive and radiative heat transfer. (Convective flow in the melt would perturb the thermal profile and is controlled by proper crucible dimensions.) Conductive heat transfer is modeled using solid three dimensional elements. Radiative transfer is represented by two node conduction links having properties appropriate to the temperatures and viewfactors involved.

The most critical portion of the heat flow problem is the evaluation of radiative loss from the melt surface to the slot. This particular radiation exchange is the primary factor which produces a given thermal profile in the melt. The correct viewfactors from the melt surface to the slot are therefore essential. Customarily the slot is represented by a series of rectangular areas for which viewfactors can be calculated analytically. However, refraction and reflection of radiation in the  $B_2O_3$  layer renders this approach invalid as Figure 20 illustrates. Therefore, an analysis of the refractive effect of the

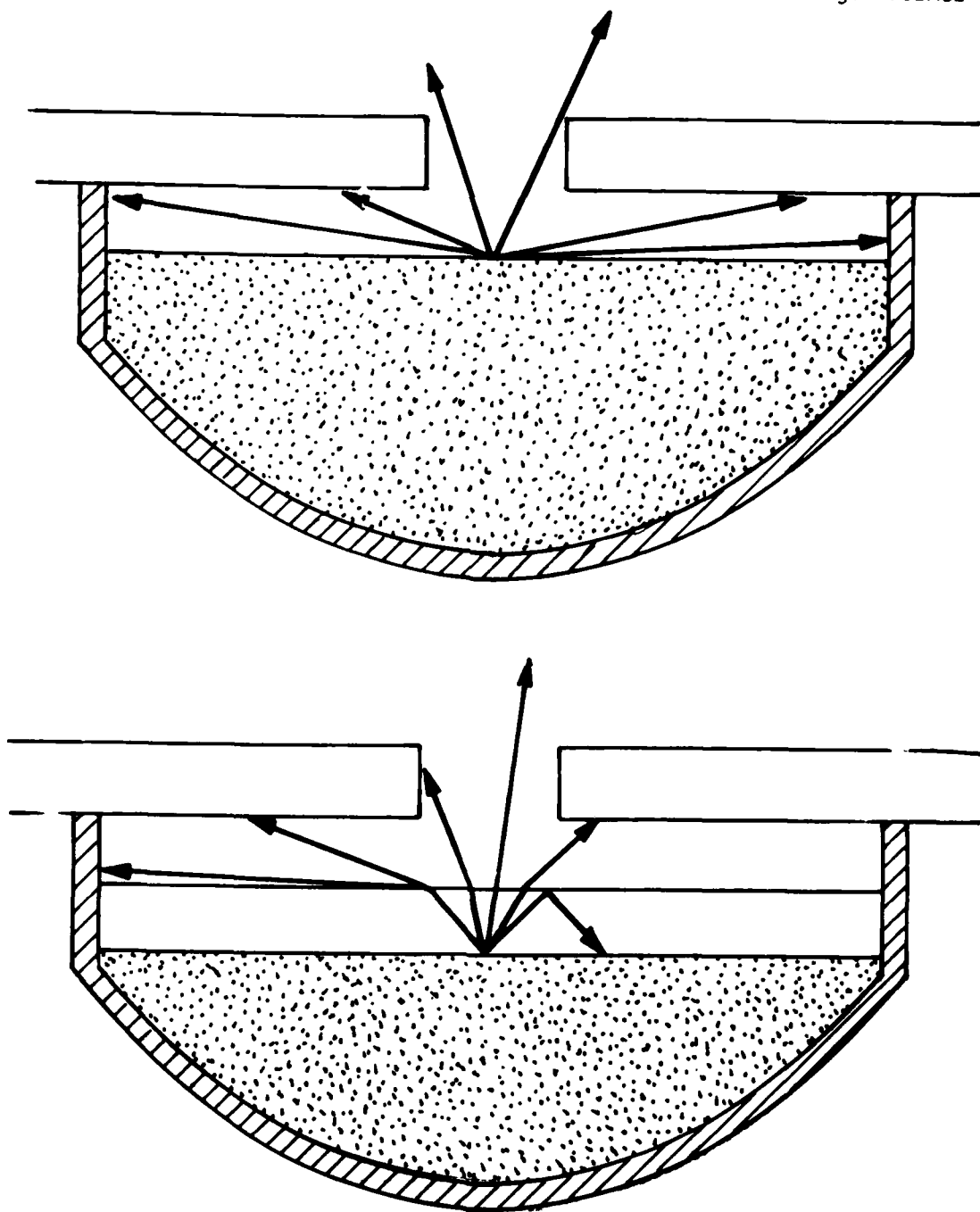


Figure 20 For the Upper Figure the Viewfactors from Points on the Melt Surface can be Calculated Analytically. The Presence of a Refracting Layer (Lower Figure) Changes the Path of the Radiation and Alters the Viewfactors to the Slot.

$B_2O_3$  was performed in order to obtain the correct viewfactors for the complete thermal analysis.

#### 3.4.2. Refraction Analysis

The intensity of radiation in a refracting medium is enhanced by  $n^2$  according to the Planck law. The total radiated power is conserved due to the counterbalancing effect of total internal reflection. The power radiated to specified areas through a refracting layer of finite thickness is not so easily deduced from first principles. Therefore, a ray tracing program was developed which delineates the path of radiation emanating from given points in the system.

The logic of the ray tracing program is shown schematically in Figure 21. Radiation from the melt surface is traced throughout the system using appropriate reflection and refraction conditions. Radiation originating at the hot lid and wall must also be analyzed in this fashion in order to obtain correct viewfactors for all radiation paths that are modified by the  $B_2O_3$ . A more detailed description of the total analysis of radiant heat transfer in the system is given in Appendix B.

#### 3.4.3 Modeling Results

The general effect of the  $B_2O_3$  layer on heat loss through the slot can be determined directly from the ray tracing program output. The total radiation from several points on the melt lying along the slot axis which escapes from a given "dogbone" slot is shown in Figure 22. As the depth of  $B_2O_3$  is increased the total heat loss through the slot is also increased. In addition, the radiation from the melt surface near the end hole of the slot is greatly enhanced at large depths of  $B_2O_3$ . Radiative loss through the slot from points on the melt surface perpendicular to the slot is modified according to Figure 23. Here cross over of the curves for points at large distances from the slot is more apparent than in the previous figure. The reduction of radiation from these points for larger  $B_2O_3$  depths illustrates the effects of refraction at large angles and total internal reflection. The overall effect of the  $B_2O_3$  on the heat flow and thermal profiles in the system cannot be deduced without the total WECAN analysis.

Dwg. 7702A33

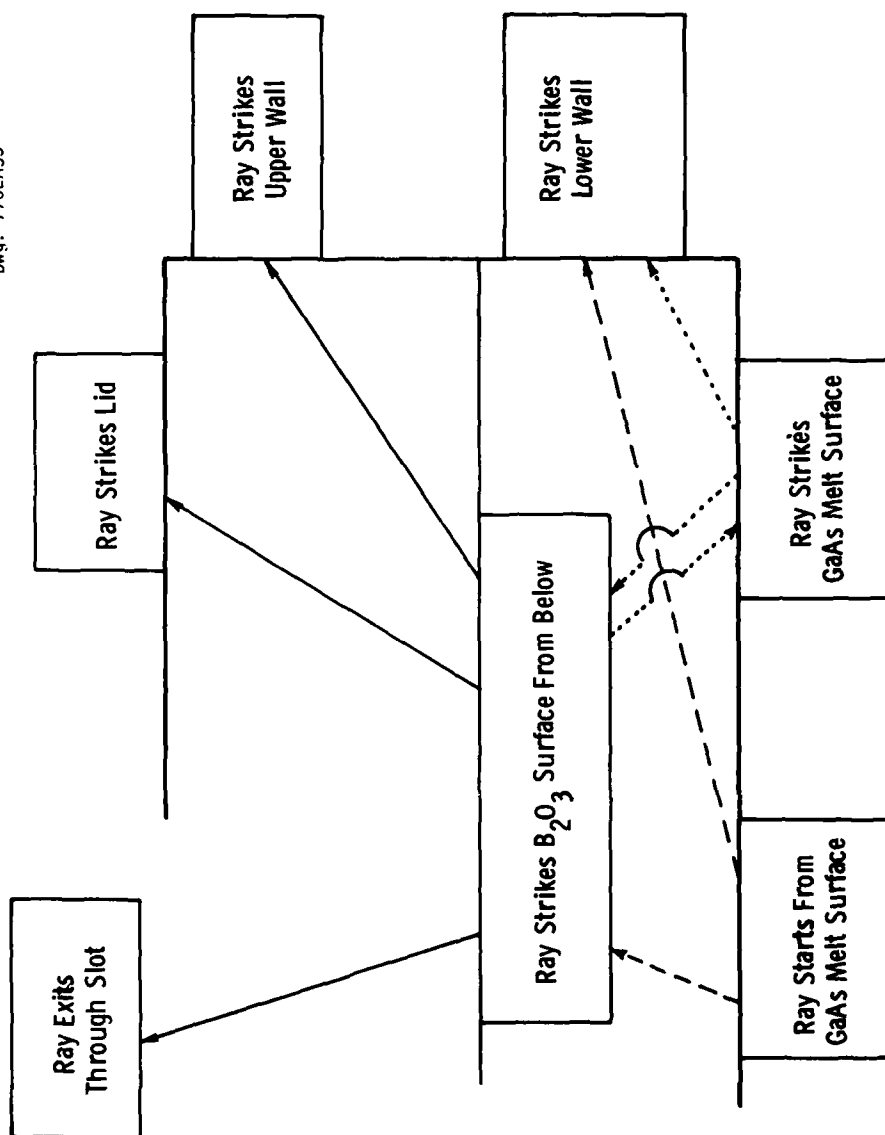


Figure 21 Schematic Diagram of the Logic of the Ray-Tracing Program. Radiation from the Melt Surface Strikes the Lower Susceptor Wall or the  $B_2O_3$  Surface. Rays Striking the  $B_2O_3$  Surface are Reflected or Refracted. Reflected Rays Undergo Total Internal Reflection Until they Strike the Lower Wall. Refracted Rays Strike the Upper Wall, the Lid, or Exit Through the Slot.

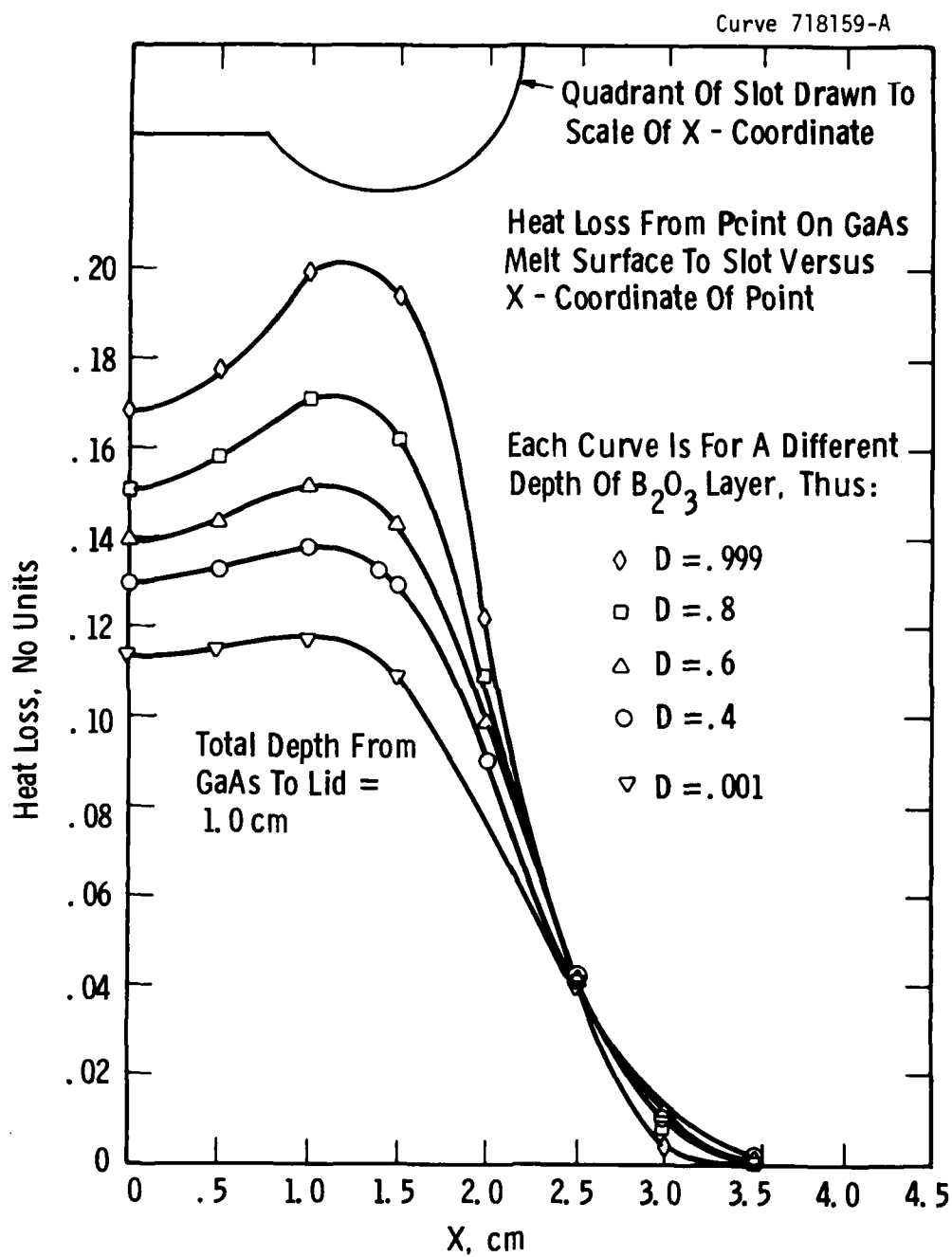


Figure 22 Heat Loss Through the Slot from Points on the GaAs Surface which Lie Under the Long Axis of the Slot. Increasing Depths of  $B_2O_3$  Increase the Radiative Loss through the Slot.

Curve 718158-A

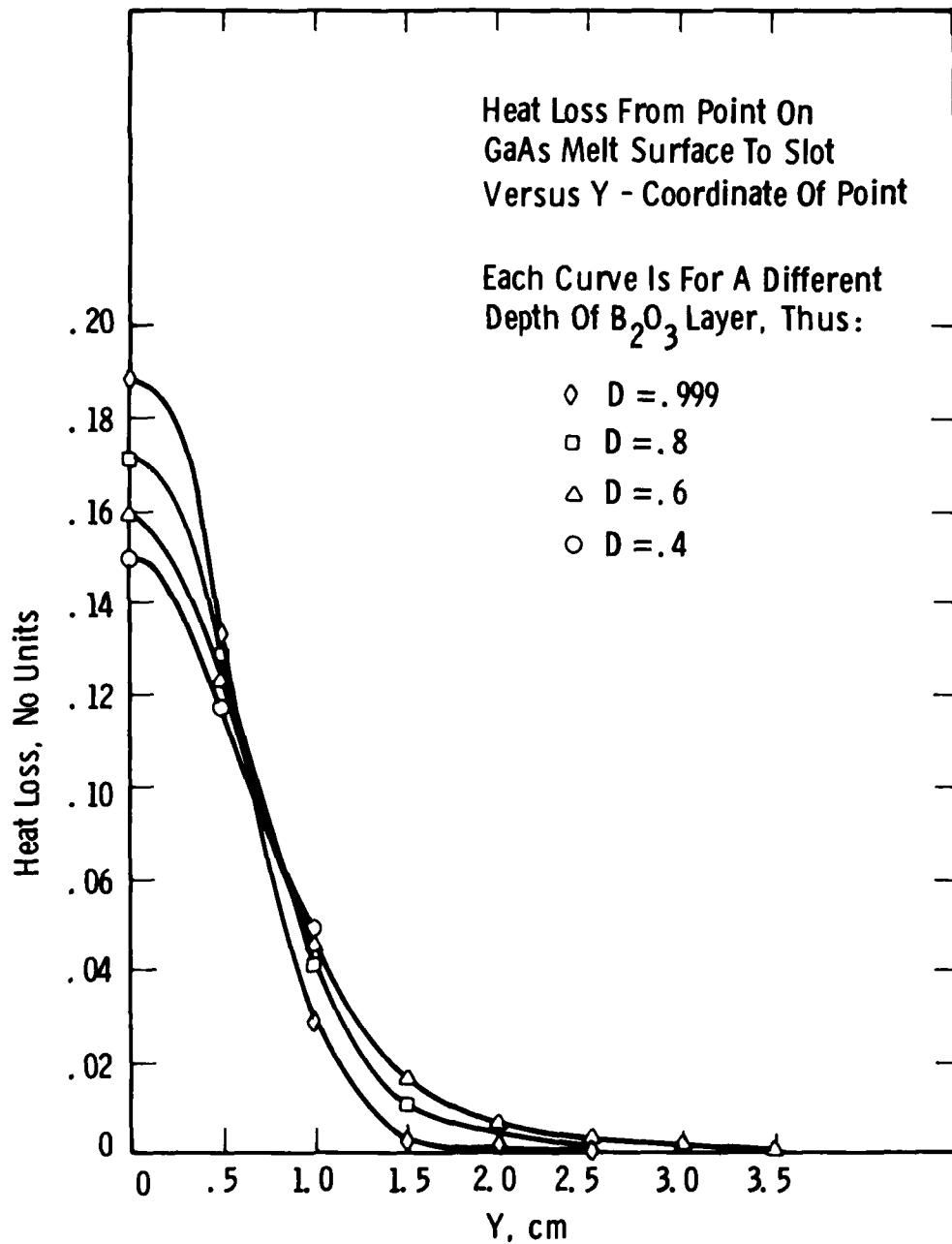


Figure 23 Heat Loss Through the Slot from Points on the GaAs Surface which Lie Perpendicular to the Slot.

The WECAN thermal model yields the temperature distribution in the system for given input conditions. The isotherms generated for one quadrant of the GaAs melt surface are given in Figure 24. The elongated isothermal region at the center is the correct thermal geometry for stable web growth.

A cross section through the melt parallel to the slot is shown in Figure 25. The inversion of the isotherms occurs at the GaAs- $B_2O_3$  interface. This indicates that a given point on the  $B_2O_3$  surface is slightly warmer than the corresponding point on the surface of the GaAs. A cross section taken perpendicular to the slot, Figure 26, illustrates the same effect.

Observation of frequent dendrite breakage at the  $B_2O_3$  surface during buttoning attempts provides experimental evidence for a thermal inversion in the  $B_2O_3$ . It is possible that the thin seed dendrites are melted in the warmer  $B_2O_3$  when the GaAs surface is at the hold temperature. The effect is detrimental to the buttoning procedure, however, elimination of the problem by simple design modifications is easily accomplished. The correlation of this observed experimental condition and the analytical results confirms the validity of the model.

The WECAN analysis has been run twice using slightly different assumptions for heat transfer between the susceptor and crucible. In both cases similar results were obtained. The thermal geometry in the melt and susceptor is analogous to that obtained for successful Si web systems. Despite the unexpected vertical thermal gradient in the  $B_2O_3$ , the thermal analysis in general substantiates the feasibility of GaAs web growth.

Curve 718164-A

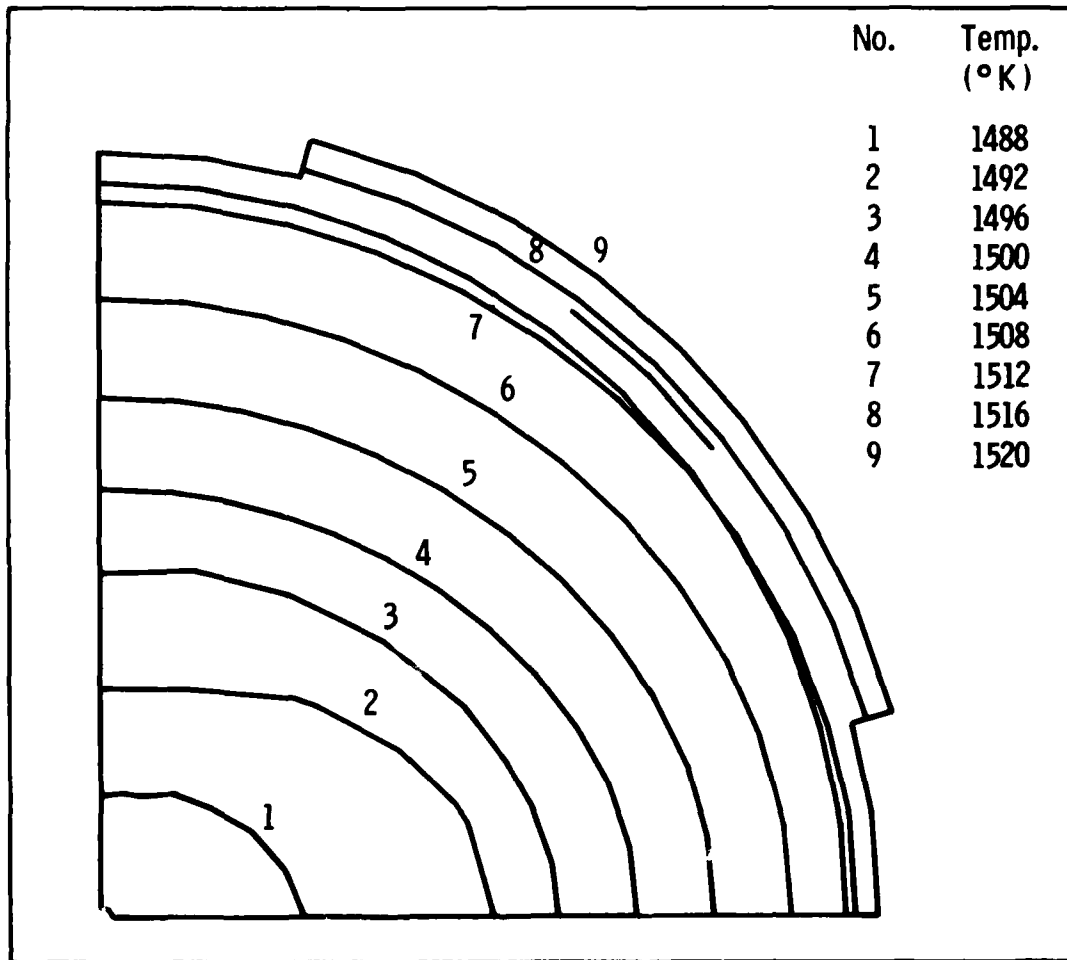
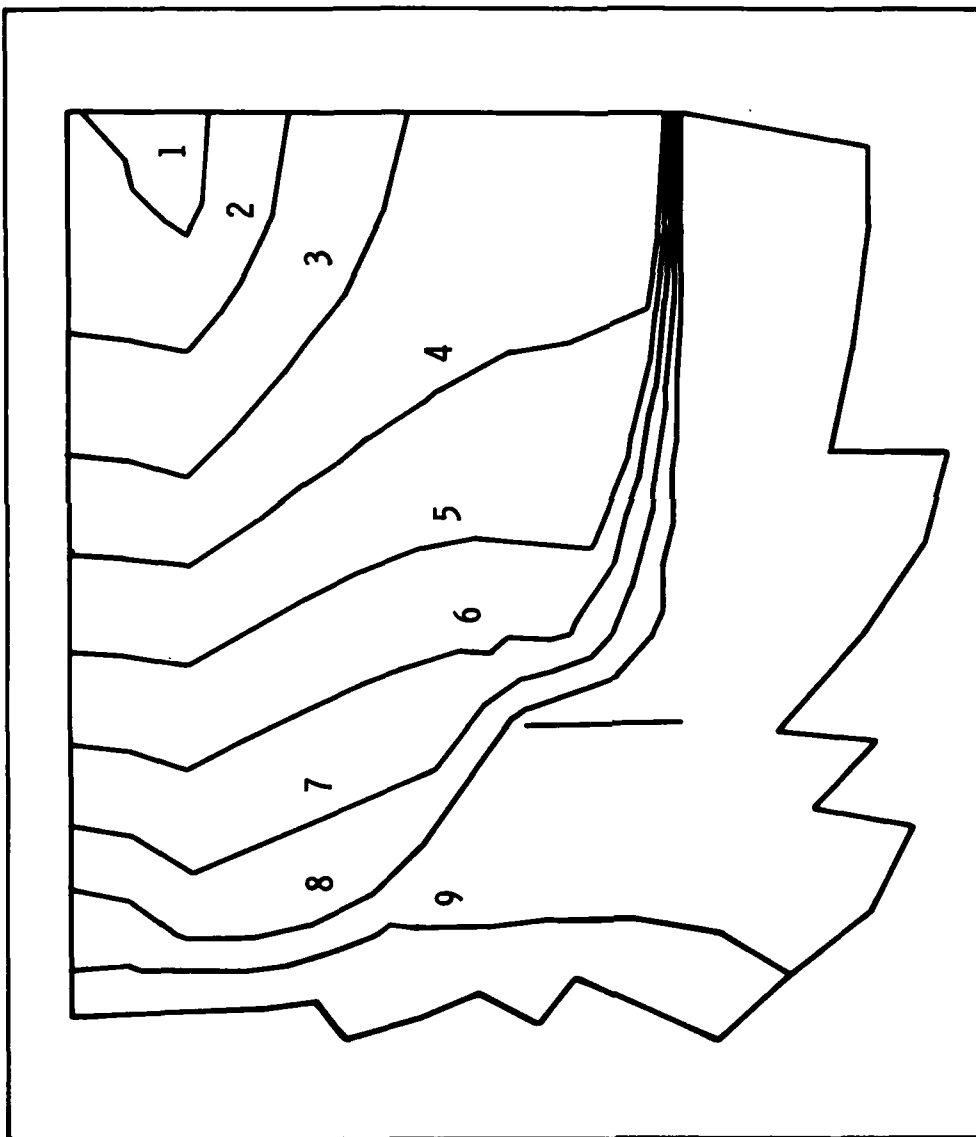


Figure 24 Isotherms Generated by the WECAN Model for One Quadrant of the GaAs Melt Surface.

Curve 718162-A



No.	Temp. (°K)
1	1488
2	1492
3	1496
4	1500
5	1504
6	1508
7	1512
8	1516
9	1520

Figure 25 WECAN Thermal Cross Section of the Melt Parallel to the Long Axis of the Slot. Inversion of the Isotherms Occurs in the  $B_2O_3$ .

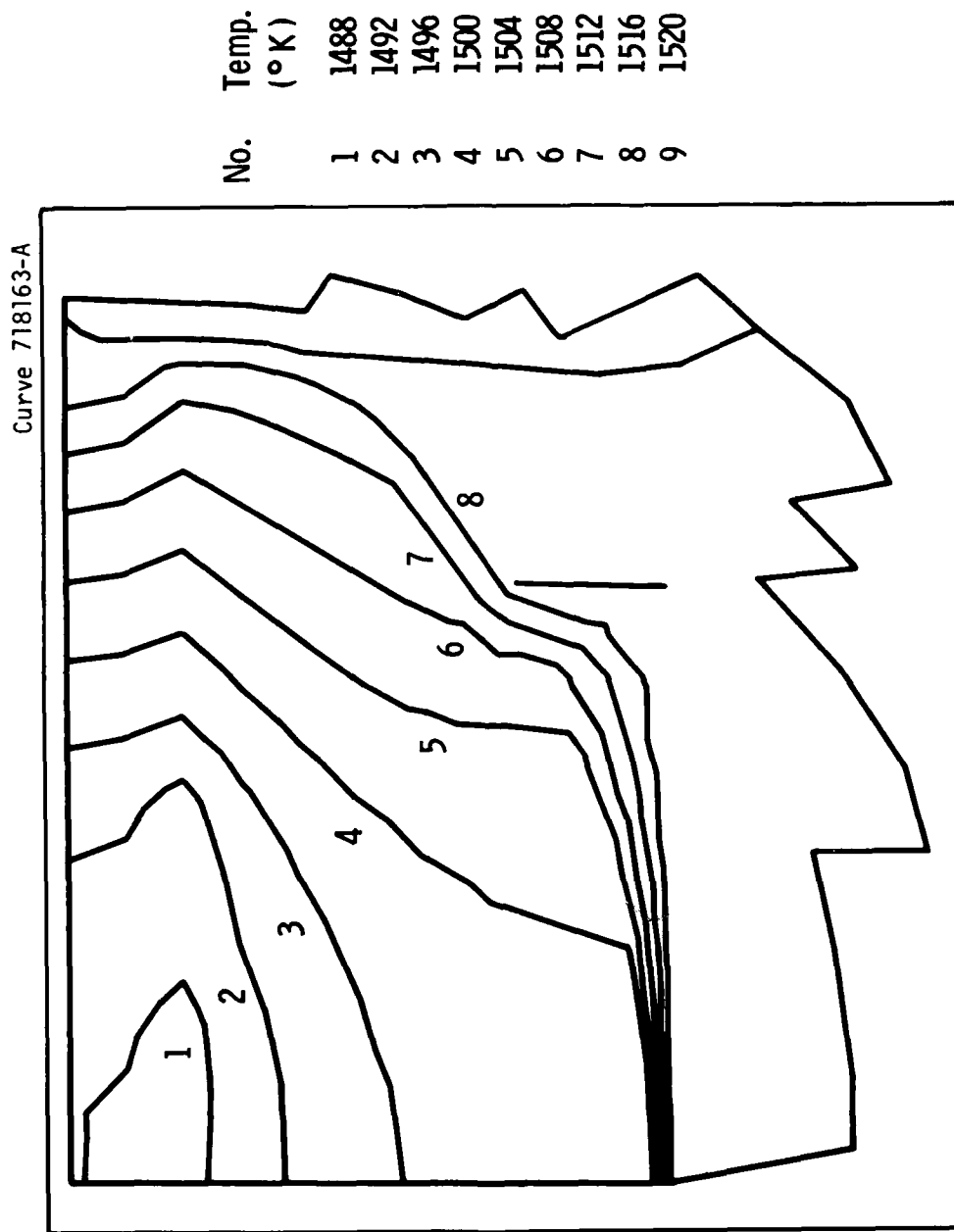


Figure 26 WECAN Thermal Cross Section of the Melt Perpendicular to the Long Axis of the Slot.

### 3.5 PROJECTED SYSTEM REFINEMENTS

#### 3.5.1 Temperature Stability

The variation of temperatures in the system during a given growth run and between successive experiments made reproducible results difficult to obtain during Phase I. Some of the apparent temperature instability can be associated with thermocouple failure. Molybdenum sheathed thermocouples fabricated by improved techniques are expected to correct this degeneration.

Another source of temperature variation is inherent in the design of the present system. Exact reproduction of thermal conditions is impossible since the susceptor is subject to small positional changes with respect to the coil during cleaning and reassembly. Slight variations in crucible fit and loading can also produce changes in heat flow. These variations cannot be eliminated, although they can be dealt with effectively using a more flexible system. Provision for lateral positioning of the susceptor with respect to the coil with the system at temperature is under investigation. Lateral coil/susceptor positioning is successfully utilized in Si web systems for required thermal trimming.

Variation of hold and growth temperatures during a given run may be due to sagging of the quartz crucible. Effects of this nature have been observed in Si systems. It was initially assumed that GaAs growth temperatures were too low to induce dimensional changes in the crucibles. However, recent experiments have shown that the crucibles in the GaAs system become soft enough to pick up the imprint of a molybdenum wire which is placed in contact with the quartz. Crucible sag changes heat transfer mechanisms to various portions of the crucible throughout a run. The temperature profile in the melt is therefore under constant modification and observed growth temperatures vary. This extended transient condition is undesirable and can be remedied by providing a very close fit between the susceptor and crucible.

The original susceptor was designed under the assumption that no crucible sag would occur. Therefore, a gap was left under the crucible (See Figure 5, Section 3.1.1) to eliminate heat transfer variations due to differences in individual crucibles. A new close fitting susceptor will be designed for future use in order to correct the temperature drift.

#### 3.5.2 Stress Reduction

The fragility and breakage of dendrites has impaired their utility as viable seeding material. Modification of handling procedures has improved their durability (See Section 3.3.).

Material stress induced by uneven distribution of  $B_2O_3$  during growth is under continuing investigation. The establishment of proper vertical thermal gradients and improved thermal symmetry in general are expected to alleviate the problem.

#### 3.5.3 System Flexibility

The modified Czochralski system used for Phase I of the program is inherently inflexible and hence impractical for systematic web growth development. Inability to remove material during a growth run severely limits the utility of the present facility. The lack of optimal coil/susceptor positioning impedes necessary thermal trimming and the short pull stroke precludes the sustained growth of web crystals.

System design changes which will be implemented in the future will remedy these conditions. The addition of an afterchamber to the furnace will facilitate product removal and seed insertion without depressurization of the system. This modification will also accommodate a new pull rod system with a longer pull stroke. The susceptor assembly will also be redesigned to eliminate crucible sagging and to improve the mechanical positioning of the susceptor with respect to the coil.

## SECTION IV

### CONCLUSIONS

The experimental and analytical results of Phase I substantiate the feasibility of GaAs web growth from a liquid encapsulated system. The growth habit and twin structure of dendrites, buttons and web material are closely analogous to Si web morphology. The behavior of basic system variables and the modeled temperature profiles also confirm the correspondence between the liquid encapsulated GaAs system and successful Si web systems.

Among the highlights of Phase I are the following accomplishments:

- Modification of the A. D. Little furnace for web growth.
- Achievement of adequate vaporization control.
- Growth and characterization of dendrites.
- Demonstration of web buttoning.
- Growth of web material.
- Analysis of  $B_2O_3$  refractive effect.
- Analysis of system temperature profiles via thermal modeling.

Several experimental difficulties have been identified during the initial phase of the program. Unstable temperatures have made reproducible results difficult to obtain. Dendrite breakage and system inflexibility have greatly limited controlled web growth experiments. However, these undesirable conditions are amenable to system refinements that are programmed for the ensuing phase of the project.

## APPENDIX A

### STANDARD OPERATING PROCEDURES

Prior to a growth run the charge of  $B_2O_3$  is vacuum dried. Trace amounts of water in the encapsulent cause vigorous bubbling which incurs As loss in a growth system. Therefore, the encapsulent must be subjected to a preliminary heat treatment. The  $B_2O_3$  is routinely dried for at least 4-6 hours at  $1000^\circ C$  and a vacuum of .04mm Hg. A 95%Pt-5% Au drying crucible is used since this alloy is not wetted by  $B_2O_3$  and the charge can be removed in tact.<sup>(9)</sup> The  $B_2O_3$  is cooled in vacuum and used immediately in order to prevent any significant rehydration of the encapsulent.

The quartz growth crucible is cleaned with aqua regia and rinsed in methanol before the charge is loaded. The seed and charge of GaAs are also etched with aqua regia. The disc of  $B_2O_3$  from the drying crucible is placed over the GaAs so that all pieces of the charge are adequately covered by the  $B_2O_3$  as it softens. Customarily 48-49gm of GaAs are used with 30gm of  $B_2O_3$ . Use of these masses in the two inch growth crucible results in a 5-6mm cover layer of  $B_2O_3$  after meltdown. The growth configuration is assembled in the A. D. Little furnace and the system is evacuated to  $1-5 \times 10^{-5}$  mm Hg overnight.

The system is pressurized to 30 psig with argon (99.985% pure) before any heat is applied. The overpressure increases to  $\sim 42$  psig at required growth temperatures.

Throughout Phase I melting was achieved as rapidly as possible, in a time of 30-45 minutes. Currently the effects of a slower meltdown are under investigation. Pull speeds vary from 10-18 cm/min for dendrites. Web growth velocities are usually near 1 cm/min.

At the end of a growth run the system is cooled rapidly by a complete power shut down. Breakage of material during cool down has been diminished by releasing the pressure once the susceptor has cooled to  $800^\circ C$ .

In the course of each growth run a powdery coating is deposited on the cool furnace walls. X-ray diffraction analysis has identified the deposit as predominantly GaAs with small amounts  $\text{As}_2\text{O}_3$  also present. The furnace is flushed with flowing argon prior to opening to reduce exposure to toxic vapors. During removal of material and cleaning, gloves and particle masks are worn. The deposit is removed by vacuuming and cleaning with methanol.

The  $\text{B}_2\text{O}_3$  must be removed from grown material before it is characterized. Removal with water causes rapid hydration and expansion of the  $\text{B}_2\text{O}_3$ . This stresses the material and induces significant damage and breakage. Removal of the  $\text{B}_2\text{O}_3$  with concentrated HF appears to incur less damage.

Samples are prepared for cross section examination by potting in Quickmount. GaAs is easily chipped and scratched by mechanical polishing. The following sequence of abrasives has been found to give the best results: 1) 600 grit wet and dry paper, 2)  $3\mu$  Microgrit, 3)  $.05\mu$  Linde B, 4) Siton. Chemical polishing is effective for removal of residual damage from mechanical polishing. The etchants utilized for chemical polishing and revealing twin planes are given in Table 5.

TABLE 5

## ETCHANTS FOR GaAs

	Composition	Ratio	Remarks
Chemical Polishing	$\text{HNO}_3:\text{HF}:\text{H}_3\text{PO}_4$	3:1:1	1-2 sec removes most polishing damage
	$\text{H}_2\text{O}_2:\text{H}_2\text{SO}_4:\text{H}_2\text{O}$	1:3:1	Fresh solution: 1-2 sec. As solution weakens up to 30 sec.
Staining Etch	$\text{CrO}_3:\text{HF}:\text{H}_2\text{O}$	1:20:20	5-15 sec.

## APPENDIX B

### ANALYTICAL TREATMENT OF RADIANT HEAT TRANSFER by E. Miksch

This appendix provides a brief outline of the method in which radiant heat transfer was represented in the thermal analysis which was performed using the Finite-Element computer code WECAN.

Due to the complexity of the WECAN model (which had 3,636 elements), it was not economically practical to iterate in order to obtain the effects of the nonlinearity in the radiative heat flow. Fortunately, it was possible to treat the radiative heat transfer by a linear approximation because the temperature differences in the system were small in comparison to the absolute temperature. Radiation from the various parts of the system is given by a  $T^4$  law. In the present analysis, the  $T^4$  curve was approximated by a straight line which is tangent to the  $T^4$  curve at the melting point of GaAs, which is 1511°K. This linear approximation was used for all aspects of the radiant heat transfer, which are discussed below.

(1) Radiation from Top of Lid

Radiation from the top of the lid was calculated, assuming a single radiation shield above the lid. No allowance was made for radiation reflected back from the environment.

(2) Radiation from O.D. of Susceptor, Lid, and Base

It was not necessary to allow for radiation from the outside diameter of the susceptor, lid, and base, because the temperatures of all nodes on these surfaces were fixed, based on experimental data.

(3) Radiation from Bottom of Base

Radiation downward from the bottom of the base was calculated, assuming six radiation shields below the base. No allowance was made for radiation reflected back from the environment.

(4) Radiation in the Space between the Lid and the GaAs Melt

Due to the highly-interactive nature of the radiative heat transfer below the lid, it was necessary to represent the heat transfer by a three-dimensional network of radiation links. In some regards, the network was analogous to a network of electrical resistors.

Radiation connections were made to each node on the GaAs melt surface, and to each element on the lid. Connections were also made to points on the vertical wall( the I.D. of the susceptor).

Due to the presence of the  $B_2O_3$  layer, it was not possible to use conventional methods to calculate view factors from one part of the system to any other part, because the top surface of the  $B_2O_3$  layer caused refraction and reflection. Hence, a ray-tracing program was written which represented what actually happens in the physical situation.

The ray-tracing program proceeded as follows: From each point on the GaAs melt surface, a large number of rays (e.g. 10,000) was defined. Each ray was then traced, first with one polarization, and then with the other polarization. When any ray encountered the top of the  $B_2O_3$  layer, both refracted and reflected rays were considered. When a ray returned to the melt surface, some of its energy was assumed to be absorbed, and some was assumed to be specularly reflected. Whenever a ray struck one of the molybdenum surfaces (wall, or underside of lid), it was considered to be absorbed. Diffuse reflection from the molybdenum was treated subsequently by using an electrical analogue.

Data representing the fraction of the energy emitted from a point on the GaAs melt surface to other parts of the system was used to define three connections to each point on the GaAs melt surface. One connection went to a node which

represented the slot (radiation lost from the system). Another connection went to a node which was connected to each element on the lid above the melt. Another connection went to a node which was connected to nodes on the wall.

The radiation links from each point on the GaAs melt surface had conductances which were proportional to the area associated with the point. These areas were calculated from the elements referencing the node. For each element face on the GaAs melt surface, its area was apportioned between the nodes it referenced in such a way that the centroid of the area values given to the nodes was in the same location as the centroid of area of the element face. These radiation conductances also included a factor for the increased radiation from the GaAs caused by the proximity of the  $B_2O_3$  as required by the index of refraction term in the Plank radiation law.

Similar calculations of radiation from other parts of the system provided values for a connection from the node connected to the lid to the node representing the slot; a connection from the node connected to the wall to the node representing the slot, and a connection between the node connected to the lid to the node connected to the wall.

A total of 430 radiation links were calculated by these methods, and they were prepared as input to the WECAN computer model.

## REFERENCES

1. "Gallium Arsenide Dendrite Single Crystal Program", Air Force Contract AF 33(657)-8162, Final Report No. MLTDR 64-129, Westinghouse Electric Corporation. (1964).
2. Richman, D., "Dissociation Pressures of GaAs, GaP, and InP and the Nature of III-V Melts", Journal of Physics and Chemistry of Solids, Volume 24, p. 1131 (1963).
3. Metz, E. P. A., Miller, R. C., and Mazelsky, R., "A Technique for Pulling Single Crystals of Volatile Materials", Journal of Applied Physics, Volume 33, p. 2016 (1962).
4. Mullin, J. B. Straughan, B. W., and Brickell, W. S., "Liquid Encapsulation Techniques: The Use of an Inert Liquid in Suppressing Dissociation During the Melt-growth of InAs and GaAs Crystals", Journal of Physics and Chemistry of Solids, Volume 26, p. 782 (1965).
5. Grabmaier, B. C. and Grabmaier, J. G., "Dislocation-Free GaAs by the Liquid Encapsulation Technique", Journal of Crystal Growth, Volume 13, p. 635 (1972).
6. Weiner, M. E., Lassota, D. T., Schwartz, B., "Liquid Encapsulated Czochralski Growth of GaAs", Journal of the Electrochemical Society: Solid State Science, Volume 118, p. 301 (1971).
7. Bass, S. J., and Oliver, P. E., "Properties of Gallium Arsenide Crystals Produced by Liquid Encapsulation Pulling", International Symposium on Gallium Arsenide, p. 41 (1966).
8. Lessoff, H. and Swiggard, H., "Research on Gunn Effect Materials (III-V Compounds)", NRL Memorandum Report 3360, Naval Research Laboratory (1976).

9. Haggerty, J. S. and Wenckus, J. F., "Development of Techniques for the Growth of Bulk Single Crystals of Several III-V Compound Semiconductors", NASA Contract No. NAS 19-2020, Report No. N70-17301, Arthur D. Little, Inc. (1969).
10. Faust, J. W., Jr., and John, H. F., "Germanium Dendrite Studies II. Lateral Growth Processes", Journal of the Electrochemical Society, Volume 108, p. 860 (1961).
11. Faust, J. W., Jr., and John, H. F., "Germanium Dendrite Studies I. Studies of Twin Structure and Seeding Mechanism", Journal of the Electrochemical Society, Volume 108, p. 855 (1961).
12. Ewing, C. T., Spann, J. R., and Miller, R. R., "Radiant Transfer of Heat in Molten Inorganic Compounds at High Temperatures", Journal of Chemical and Engineering Data, Volume 7, p. 246 (1962).